communications biology

A Nature Portfolio journal

Article

https://doi.org/10.1038/s42003-025-08255-w

Deacetylation of nuclear AIF provides a braking mechanism for caspase-independent chromatinolysis and necrotic brain injury

Chen Hu[1,6], Jichuan Geng[1,6], Peipei Shan[2], Tongqing Zhang[1], Zhuqing Zhang[1], Xiaoyu Zhang[1], Menghan Lin[1], Xiaoxia Zhang[1], Dong Chang[1], Baokun He[3], Deshui Jia[4], Mary Zhang[5], Chuangui Wang[1] ✉ & Shengping Zhang[1] ✉

Programmed necrosis involves three consecutive stages: initiation, propagation, and execution. The initiation of necrosis has been widely studied, but due to the diversity and pleiotropy of the initiating pathways, it is difficult to identify ideal targets for necrosis inhibition from upstream necrosis pathways. Genetic evidence suggests that caspase-independent chromatinolysis, an execution process in multiple forms of necrosis, could be targeted to inhibit necrosis, but its regulatory mechanisms remain unclear. Previous studies suggest that the apoptosis-inducing factor AIF promotes chromatinolysis and caspase-independent necrosis, and its cytosol-to-nucleus translocation induces irreversible chromatinolysis. Here we report that AIF acetylation at lysine 295 is required for its cytosol-to-nucleus translocation and conduction of caspase-independent chromatinolysis upon necrotic stimuli, the SIRT1 deacetylase blocks necrotic chromatinolysis via deacetylating AIF, and pharmacological activation of SIRT1 inhibits AIF-dependent chromatinolysis and necrotic brain injury. Our results reveal a reversible blocking mechanism for AIF-dependent chromatinolysis and caspase-independent necrosis, supporting that targeting the late necrosis stage is a promising therapeutic strategy for treatment of necrosis-associated diseases.

Necrosis was previously viewed as accidental and unregulated cell death; however, accumulating evidence indicates that many types of necrotic cell death (*e.g., necroptosis, pyroptosis, parthanatos, ferroptosis, NETosis*, and *pyronecrosis*) can be regulated. These types of necrosis are defined as programmed necrosis[1,2]. Programmed necrosis has attracted attention for its critical role in various pathological conditions, such as stroke, neurodegenerative diseases, organ ischemia-reperfusion injury, microbial infections, inflammation, and autoimmune diseases[1–3]. The mechanistic steps of different programmed necrosis pathways can be classified into four levels: triggers, initiators, mediators, and executioners[1]. Accumulating research reveals that programmed necrosis exhibits greater mechanistic redundancy and diversity at the trigger and initiation levels compared to downstream levels. For example, PARP-1 activation is essential for initiating parthanatos[4], and its inhibition has been shown to suppress parthanatos[5]. However, PARP-1 also plays a critical role in sensing DNA breaks and facilitating DNA repair through multiple pathways[6], which may induce cytotoxicity and potential long-term adverse effects when targeting PARP-1 to suppress parthanatos. Thus, targeting downstream executioners will be more efficient to treat programmed necrosis-associated diseases.

On the other hand, growing evidence indicates that inhibiting the execution process of specific forms of programmed necrosis can effectively suppress this type of cell death[1,7–9]. Therefore, targeting downstream

[1]Biomedical Research Institute, School of Life Sciences and Medicine, Shandong University of Technology, Zibo, 255049, China. [2]Institute of Translational Medicine, The Affiliated Hospital of Qingdao University, College of Medicine, Qingdao University, 38 Dengzhou Rd, Qingdao, 266021, China. [3]Institute of Chinese Materia Medica, The Fourth Clinical Medical College, Guangzhou University of Chinese Medicine, Shenzhen, Guangdong, 518033, China. [4]Laboratory of Cancer Genomics and Biology, Department of Urology, Shanghai General Hospital, Shanghai Jiao Tong University School of Medicine, Shanghai, 201620, China. [5]Department of Oncology, Karmanos Cancer Institute, Wayne State University School of Medicine, 4100 John R, Detroit, MI, 48201, USA. [6]These authors contributed equally: Chen Hu, Jichuan Geng. ✉e-mail: cgwang24@sdut.edu.cn; spzhang@sdut.edu.cn

executioners could offer a more precise and effective therapeutic strategy for inhibiting programmed necrosis, with reduced off-target effect. The apoptosis-inducing factor AIF serves as a pivotal executioner of programmed necrosis, which is induced by factors such as alkylating DNA damage, hypoxia/ischemia, and NMDA/glutamate exposure[5,7,10–12]. Upon release from the mitochondria into the cytosol in response to necrotic stress, AIF translocates to the nucleus, where it initiates irreversible chromatinolysis[13]. Inhibition of the AIF-associated PAAN/MIF nuclease suppresses programmed necrosis and neurodegeneration induced by α-synuclein preformed fibrils (PFFs), adeno-associated virus (AAV)-mediated α-synuclein overexpression, and MPTP (1-methyl-4-phenyl-1,2,3,6-tetrahydropyridine) intoxication in vivo[14]. Therefore, focusing on the execution stage of programmed necrosis may be a more effective strategy for inhibiting programmed necrosis and its associated diseases. However, the molecular mechanisms regulating this execution stage are not yet fully understood.

SIRT1, an NAD^+-dependent deacetylase, plays crucial roles in multiple cellular processes, including stress responses, cellular metabolism, and gene transcription[15–18]. For instance, SIRT1 deacetylates p53[19], E2F1[20], and FOXO1[17], thereby repressing apoptosis and promoting cell survival. Our previous study identified several SIRT1-interacting proteins, including E2F1[20], PABP1[21], and REGγ (PA28γ)[22] through mass spectrometry analysis of the proteins co-precipitated with SIRT1. Interestingly, we also observed that the mitochondrial protein AIF is a potential SIRT1-binding protein. AIF is known to be essential in PARP-1-dependent cell death (parthanatos). PARP-1 and SIRT1 are two enzymes that rely on NAD and are pivotal in determining whether a cell survives or dies under stress. Previous research has reported the interplay between these two proteins[23]. SIRT1 inhibits PARP-1 activity upon DNA damage, and SIRT1 deficiency leads to PARP-1 overactivation-induced AIF-mediated apoptosis following H_2O_2 treatment[24]. SIRT1 may downregulate PARP-1 activity both through deacetylating PARP-1 and by repressing the synthesis of the PARP-1 protein via its gene promoter[25]. Additionally, SIRT1 might contribute to parthanatos by initiating NAD depletion, resulting in the upregulation of NOX2 and NAT10[26]. However, neither the evidence for direct interaction between SIRT1 and PARP-1 nor the significance of this effect in vivo was found. Additionally, various studies have revealed that AIF participates in the regulation of necroptosis, parthanatos, and ferroptosis[5,7,13,27], and its nuclear translocation leads to irreversible chromatinolysis and necrotic cell death[7,13,28]. Upon the induction of cell death, AIF is released from the mitochondria and translocates to the nucleus from the cytoplasm[29]. Cyclophilin A (CypA) regulates the cytosolic-nuclear transition of AIF[30], while HSP70, as an inhibitor of this process, facilitates the anti-apoptotic effect[31]. In the nucleus, AIF participates in chromatin condensation and DNA degradation by interacting with DNA in a sequence-independent manner[32]. Since AIF lacks intrinsic nuclease activity, it primarily recruits non-specific endonucleases, such as CypA[33], MIF[34], to cleave DNA. Concurrently, AIF interacts with γH2AX to form a DNA degradation complex with CypA or MIF within the chromatin, thereby facilitating chromatinolysis[34,35]. Given that SIRT1 is mainly distributed in the nucleus, we propose that SIRT1 may interact with the nuclear-translocated AIF and thus provide a braking mechanism for AIF-mediated irreversible chromatinolysis. An in-depth study of the mechanisms controlling the late execution stage of necrosis is imperative for the identification of drug targets for necrosis-related diseases.

Results

SIRT1 blocks necrotic stress-induced chromatinolysis

To determine whether SIRT1 participates in the regulation of necrosis in vivo, wild-type and *Sirt1* knockout mice were subjected to unilateral middle cerebral artery occlusion (MCAO) without reperfusion as previously reported[36], in which necrosis plays a significant role in neuronal cell death[3,5,37]. A previous study reported that occlusion only causes slight ischemic cell change after 1 h, whereas occlusion for >3 h could cause severe ischemic lesions[38,39]. In this study, the wild-type (*Sirt1*-WT) and *Sirt1* knockout (*Sirt1*-KO) mice were exposed to MCAO (Fig. 1A). The infarct volume ratio following MCAO in *Sirt1*-KO mice increased by about 50% ($p < 0.01$) compared to their wild-type (WT) counterparts (Fig. 1B–D). Subsequently, brain tissues obtained from the occluded hemispheres of both wild-type and *Sirt1*-KO mice subjected to MCAO were extracted for further analysis. The brain tissues of wild-type mice exhibited minimal terminal deoxynucleotidyl transferase dUTP nick end labeling (TUNEL) staining and negligible alterations in nuclear morphology, whereas the tissues of *Sirt1*-KO mice displayed pronounced TUNEL staining and chromatin condensation (Fig. 1E), indicative of heightened cell death in *Sirt1*-KO mice under conditions of ischemic stress. Consistently, a significant increase in large-scale DNA fragmentation (~50 kb), a hallmark of AIF-mediated programmed cell death[13,29], was observed in brain samples of *Sirt1*-KO mice (Fig. 1F). Notably, previous studies have shown that the outcome of the MCAO mouse model is sex-dependent[40]. Thus, we conducted additional experiments involving both male and female wild-type and *Sirt1*-KO mice subjected to MCAO. The findings indicate that *Sirt1* depletion results in a larger infarct volume in both male and female mice compared to their wild-type counterparts of the same sex ($p < 0.01$; Fig. S1). Of note, the female *Sirt1* knockout mice exhibit a slight decrease in brain injury following MCAO treatment compared to the male *Sirt1*-KO mice. Subsequently, to validate the involvement of SIRT1 in AIF-mediated necrosis, we examined the levels of cell death in SIRT1 knockdown and control cell lines treated with N-methyl-N′-nitro-N-nitrosoguanidine (MNNG) (20 min incubation, followed by removal), a DNA alkylating agent known to induce large-scale DNA fragmentation and programmed necrosis in a caspase-independent manner[41–43]. PI/Annexin V, cell viability, and TUNEL assays demonstrated that the knockdown of SIRT1 resulted in a significant increase in cell death and reduction in cell viability following MNNG treatment (Fig. 1G–L). It has been established that programmed necrosis induced by DNA alkylating agents, such as MNNG, is caspase-independent and characterized by large-scale DNA fragmentation[34,42]. Therefore, we hypothesized that SIRT1 negatively regulates caspase-independent chromatin degradation. Consistently, pulsed-field gel electrophoresis showed that SIRT1 knockdown markedly increased the level of large-scale DNA fragmentation (~50 kb) in a time-dependent manner following MNNG treatment (20 min incubation, then removed) (Fig. 1M). Moreover, the direct inhibition of SIRT1 using its specific inhibitor, Sirtinol, resulted in a significant increase in cell death and a decrease in cell viability following MNNG treatment (Fig. 1N–P). Taken together, these results suggest that SIRT1 inhibits chromatinolysis and programmed necrosis in response to necrotic stimuli.

SIRT1 interacts with AIF in the nucleus upon necrotic stimuli

AIF facilitates necrotic chromatinolysis by mediating DNA degradation complex formation[10,13,33,34,42]. As a mitochondrial flavoprotein, AIF plays an essential role in healthy mitochondrial metabolism through its NADH oxidoreductase activity and its ability to maintain respiratory chain assembly and stability[44,45]. Upon necrotic stimuli (such as with alkylating DNA damage agents, hypoxia/ischemia, NMDA/glutamate), AIF is released from the mitochondria and translocates into the nucleus, inducing necrotic chromatinolysis and cell death by activating the nuclear DNA degradation complex composed of AIF, MIF, CypA, and γH2AX[7,34]. Necrotic stimuli, such as MNNG, trigger programmed necrosis through the activation of PARP-1, which redistributes AIF from the mitochondria to the nucleus to promote chromatinolysis[46]. Oxygen and glucose deprivation (OGD) treatment also induces the nuclear translocation of AIF[47]. Given that SIRT1 is predominantly localized in the nucleus, we postulate that necrotic stress may prompt its interaction with AIF in the nucleus. As expected, we observed the co-localization of AIF with SIRT1 in defined nuclear areas following treatment with MNNG or OGD (Fig. 2A). Additionally, results from endogenous immunoprecipitation experiments indicated that AIF interacts with SIRT1 in the nuclear fraction after exposure to MNNG or OGD (Fig. 2B–C). Meanwhile, following treatment with MNNG or OGD, SIRT1 binds to γH2AX but not to MIF (Fig. S2). In addition, the GST (glutathione S-transferase) pull-down assay confirmed the direct binding of

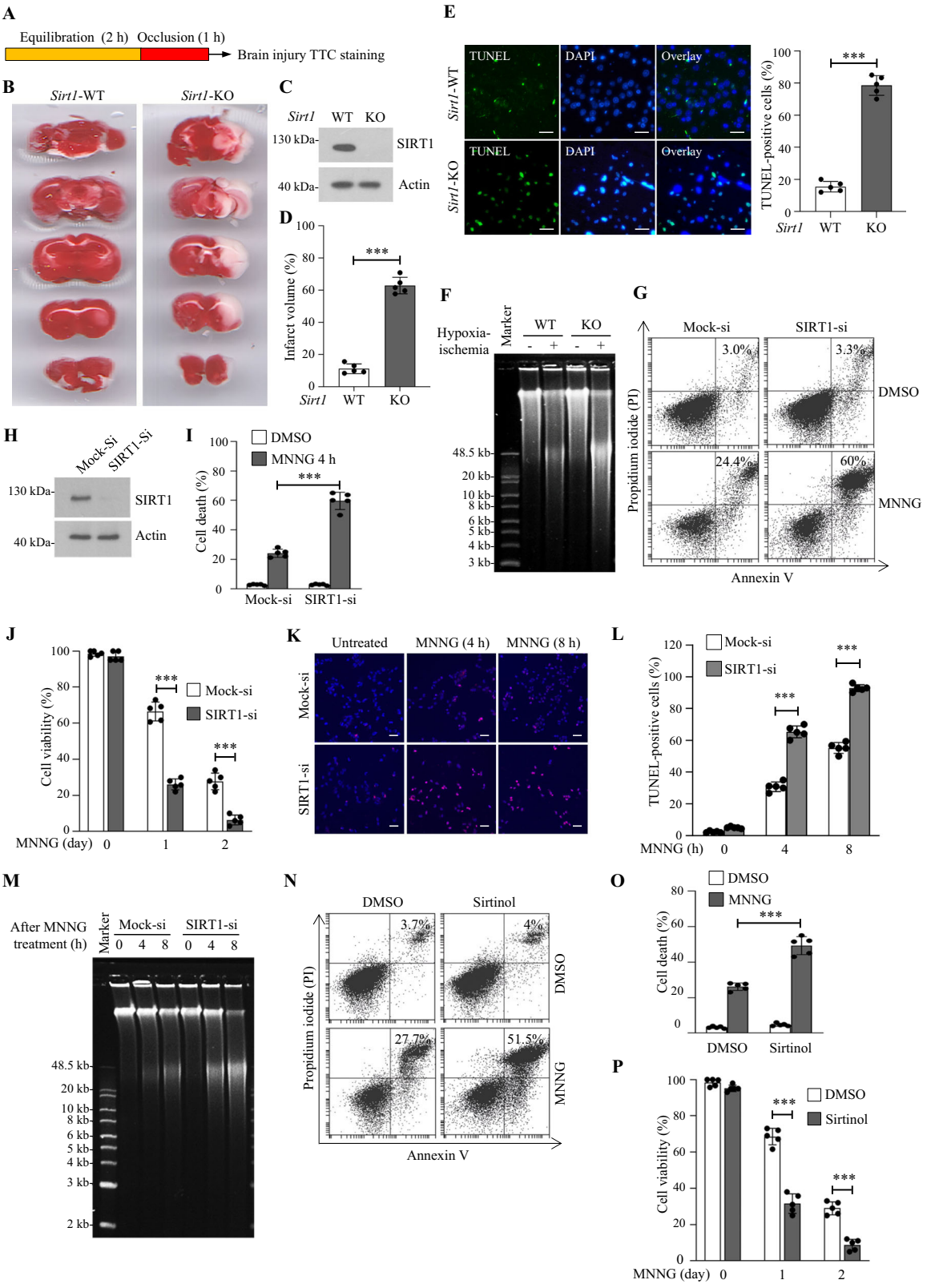

SIRT1 and AIF in vitro (Fig. 2D). Furthermore, we used SIRT1 and AIF deletion mutants to confirm the SIRT1-AIF interaction. The results showed that the region (amino acids 214-541) within the catalytic domain of SIRT1 is essential for its interaction with AIF, and that both the NADH (amino acids 263–400) and FAD (amino acids 400-480) binding domains of AIF are necessary for its interaction with SIRT1 (Fig. 2E, F). These data presented above demonstrate that treatment with MNNG or OGD induces nuclear translocation of AIF and leads to its interaction with SIRT1.

Next, we tested whether SIRT1 inhibits MNNG- or OGD-induced cell death in an AIF-dependent manner using transient knockdown of AIF and SIRT1, either singly or in combination, in SK-N-SH cells. The results showed that SIRT1 knockdown significantly increased MNNG-induced cell

Fig. 1 | SIRT1 blocks necrotic stress-induced chromatinolysis. A Strategy for establishing middle cerebral artery occlusion (MCAO) in wild-type (WT) mice and *Sirt1* knockout (KO) mice. **B** Effect of genetic depletion of *Sirt1* on the infarct volume after 1 h MCAO. The infarct size was measured by triphenyl tetrazolium chloride (TTC) staining demonstrate a significant increase of infarcted brain tissue in *Sirt1*-KO mice compared with *Sirt1*-WT littermate controls. **C** Western blot analysis of SIRT1 protein in the brain of WT and *Sirt1* knockout (KO) mice. **D** Infarct size was evaluated histomorphometrically on consecutive TTC-stained brain sections throughout the infarct. The data represent the means of five independent experiments ($n = 5$) ± SD and are shown in each column. ***$p < 0.01$. **E** Representative images of TUNEL (green) and DAPI (blue) staining in the brain penumbra area from sham and MCAO-exposed mice after ischemia. Scale bars indicate 20 μm. On the right panel, the frequency of TUNEL-positive labeling (% cell death) in (**E**) was counted and plotted as a percentage of total cells. The data represent the means of five independent experiments ($n = 5$) ± SD and are shown in each column. ***$p < 0.01$. **F** Large-scale DNA fragmentation (~50 kb) was determined by gel electrophoresis in the penumbra area after 1 h of MCAO surgery in *Sirt1*-WT and *Sirt1*-KO mice. **G–I**Scramble siRNA (Mock-si) or siRNA against human SIRT1 (SIRT1-si) was transfected into SK-N-SH cells. 48 h after the indicated transfection, the cells were treated with DMSO or MNNG (4 h), labeled with Annexin-FITC and PI, and analyzed by flow cytometry (**G**), western blot analysis of SIRT1 expression in the scramble siRNA (Mock-si) and specific siRNA (SIRT1-si) against SIRT1 (**H**), and the frequency of double-positive labeling cells was recorded and expressed as a percentage (**I**). The data represent the means of five independent experiments ($n = 5$) ± SD and are shown in each column. ***$p < 0.01$. **J** Scramble siRNA (Mock-si) or siRNA against human SIRT1 (SIRT1-si) was transfected into SK-N-SH cells. 48 h after the indicated transfection, the cells were treated with DMSO or MNNG. A CCK-8 assay was performed to measure cell viability after the treatment as indicated time. The data represent the means of five independent experiments ($n = 5$) ± SD and are shown in each column. ***$p < 0.01$. **K-L** Indicated siRNA-transfected SK-N-SH cells were untreated (0 h) or treated with MNNG, stained for the detection of 3'-OH DNA breaks (TUNEL, red), and visualized using fluorescent microscopy. DAPI (blue) was used to visualize the nuclei. Representative overlay images are shown in (**K**), scale bars indicate 50 μm. And the frequency of TUNEL-positive labeling (% cell death) was counted and plotted as a percentage of total cells. The data represent the means of five independent experiments ($n = 5$) ± SD and are shown in each column (**L**). ***$p < 0.01$. **M** Large-scale DNA fragmentation induced by MNNG. SK-N-SH cells were transiently transfected with siRNA for 2 days, then treated with MNNG and subjected to nuclear DNA extraction. Pulsed-field gel electrophoresis was used to visualize large-scale DNA fragments. For MNNG treatment, cells were incubated with a culture medium containing 500 μM MNNG for 20 min, then washed three times with PBS and re-cultured for a further 4 or 8 h in fresh medium without MNNG. **N-O** SK-N-SH cells were pre-treated with SIRT1-specific inhibitor Sirtinol (50 μM) for 12 h. Then, cells were subjected to DMSO or MNNG treatment. 4 h after treatment, cells were labeled with Annexin V-FITC and PI and subsequently analyzed via flow cytometry (**N**), and the frequency of Annexin V and PI-positive labeling (% cell death) was recorded by flow cytometry and illustrated in the figure (**O**). The data represent the means of five independent experiments ($n = 5$) ± SD and are shown in each column. ***$p < 0.01$. **P** SK-N-SH cells were pre-treated with the SIRT1-specific inhibitor Sirtinol (50 μM) for 12 h. Then, cells were subjected to DMSO or MNNG treatment. After the treatment, a CCK-8 assay was performed to measure cell viability as indicated time. The data represent the means of five independent experiments ($n = 5$) ± SD and are shown in each column. ***$p < 0.01$.

death, whereas double knockdown of AIF markedly downregulated this effect (Fig. S3A–C). Similar results were observed under OGD-treated cells (Fig. S3D–E). Moreover, inhibition of SIRT1 with Sirtinol significantly increased MNNG-induced cell death, while transient knockdown of AIF by siRNA mitigated this effect (Fig. S3F–G). These results indicate that SIRT1 inhibits MNNG- or OGD-induced cell death in an AIF-dependent manner. By integrating the aforementioned data with the observation that the depletion or inhibition of SIRT1 leads to increased necrotic stress-induced large-scale DNA fragmentation and cell death (Fig. 1), we conclude that SIRT1 functions as a nuclear protector against AIF-mediated necrosis under necrotic conditions.

AIF is acetylated under stress conditions

Given that SIRT1 functions as an NAD^+-dependent deacetylase, the interaction between AIF and SIRT1 prompts us to examine if AIF is a target of SIRT1. To explore this possibility, we initially investigated whether AIF could be modified by acetylation. As expected, MNNG or OGD treatment induced AIF acetylation (Fig. 3A, B). Furthermore, the overexpression of p300 or CBP acetyltransferases in 293 T cells led to an increase in AIF acetylation under normal or MNNG treatment conditions (Fig. 3C). Next, we examined the spatio-temporal dynamics of AIF acetylation under necrotic conditions. SK-N-SH cells were challenged with MNNG for 0–12 h or subjected to OGD for 0–24 h, and then cell extracts were separated into nuclear (N) and post-nuclear (PN) fractions and analyzed by western blotting. Results showed that MNNG or OGD treatment promoted cytosolic and nuclear acetylation of AIF in a time-dependent manner (Fig. 3D–E), suggesting that AIF acetylation is associated with its nuclear translocation.

SIRT1 deacetylates AIF under necrotic stress conditions

Next, we examined whether endogenous SIRT1 deacetylates AIF under necrotic conditions. Results showed that transient knockdown of SIRT1 increased MNNG- and OGD-induced AIF acetylation in the nucleus (Fig. 3F). Moreover, the SIRT1 activator SRT1720 treatment markedly inhibited acetylation of AIF after MNNG or OGD treatment, whereas inhibition of SIRT1 by Sirtinol increased AIF acetylation (Fig. 3G). To confirm that the deacetylase activity of SIRT1 is required for AIF deacetylation, we co-transfected AIF with either SIRT1-WT or a catalytic-deficient mutant of SIRT1 (SIRT1-H363A) in 293 T cells. Results showed that overexpression of SIRT1-WT, but not SIRT1-H363A, markedly repressed MNNG-induced AIF acetylation (Fig. 3H). Next, we used purified *E. coli*-expressed GST-tagged SIRT1 protein and FLAG-tagged AIF protein, which immunoprecipitated from the 293 T cells, to perform In vitro deacetylation assays. Results showed that SIRT1-WT, but not SIRT1-H363A, deacetylates AIF in an NAD-dependent manner (Fig. 3I). Collectively, these data suggest that SIRT1 deacetylates AIF under necrotic stress.

AIF-K295 acetylation is required for chromatinolysis and programmed necrosis

To identify potential acetylation sites on AIF, we transiently transfected 293 T cells with AIF-Flag overexpression plasmids. Approximately 24 h post-transfection, the cells were treated with or without MNNG for an additional 12 h. Subsequently, the cells were harvested and subjected to immunoprecipitation using FLAG-M2 beads (Fig. 4A). The immunoprecipitated samples were then analyzed via mass spectrometry. We found that the AIF lysine 295 (K295) is a potential acetylation site after MNNG treatment (Fig. 4B). Notably, acetylation data recorded in the protein modification database PhosphoSitePlus suggest that AIF has four potential acetylation residues: K231, K232, K295, and K593. Therefore, we mutated each lysine residue to arginine (K231R, K232R, K295R, or K593R) and determined the acetylated residue under MNNG treatment. The results showed that the AIF-K295R mutant, but not the other K to R mutants, lost most of its acetylation ability (Fig. 4C). These results suggest that lysine 295 is the major acetylation site of AIF. Moreover, lysine 295 of AIF is evolutionarily conserved among mammals (Fig. 4D).

Next, we generated an antibody specific for recognizing the acetylated lysine 295 of AIF(AIF-K295^{ac}). To test the specificity of this antibody, the ectopically expressed wild-type AIF, acetylation-deficient K295R or acetylation-mimicking K295Q AIF were immunoprecipitated from the MNNG-treated 293 T cells, and then subjected them to western blot analysis using the AIF-K295^{ac} antibody. Results showed that only the wild-type AIF (acetylated upon MNNG treatment), but not the K295R and K295Q mutants of AIF, was recognized by this antibody (Fig. 4E), indicating that the antibody is highly specific to AIF-K295^{ac}. To test the role of endogenous SIRT1 in deacetylation of AIF-K295^{ac}, we examined

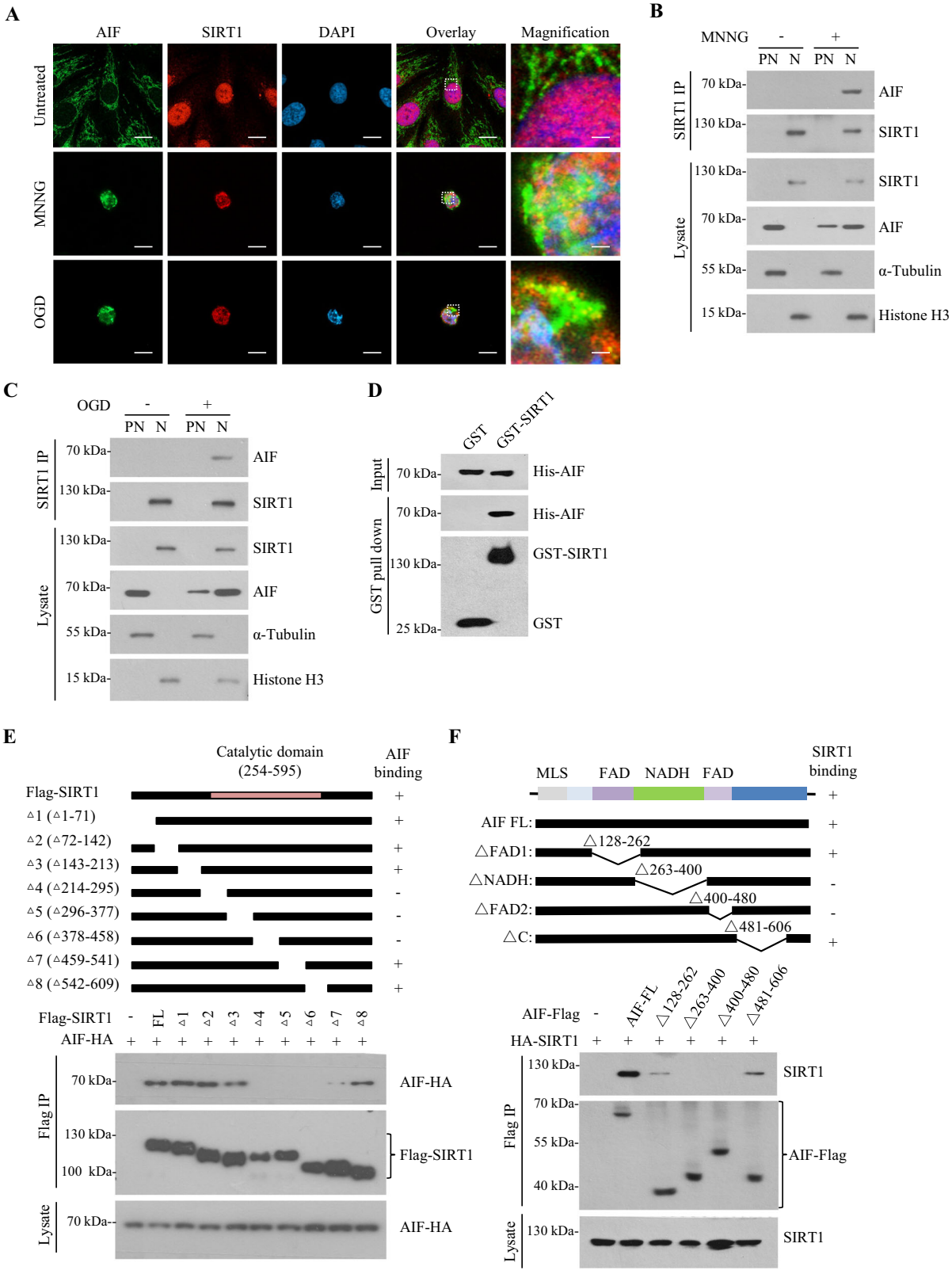

the AIF-K295^{ac} in SK-N-SH cells that were treated with MNNG or OGD. These cells included control shRNA (shN) and SIRT1-specific shRNA stable-expressing (shR) variants. We observed that stable ablation of SIRT1 markedly enhanced stress-induced AIF-K295^{ac} in the nucleus (Fig. 4F). This indicates that SIRT1 is required for nuclear deacetylation of AIF-K295^{ac} under stress conditions. Of note, SIRT2 deacetylase is predominantly localized in the cytosol; however, it can transiently translocate to the nucleus in a cell cycle-dependent manner[48], we therefore also examined the possibility of SIRT2 in the regulation of AIF-K295^{ac}. The results showed that SIRT2 is unable to deacetylate AIF-K295^{ac} following MNNG treatment (Fig. S4), supporting the notion that SIRT1 specifically deacetylates AIF-K295^{ac} under stress conditions.

Fig. 2 | SIRT1 interacts with AIF in the nucleus. A SK-N-SH cells treated with MNNG (12 h) or OGD (12 h) were stained for AIF (green) and SIRT1 (red) and viewed using confocal fluorescence microscopy. Nuclei were stained with DAPI (blue). Scale bars indicate 10 μm. Magnification scale bars indicate 1 μm. **B**, **C** Binding of AIF and SIRT1 under MNNG or OGD treatment. For MNNG treatment, cells were incubated with a culture medium containing 500 μM MNNG for 20 min, then washed three times with PBS and re-cultured for an additional 12 h in fresh medium without MNNG. For OGD treatment, cells were placed in an I-CONIC hypoxic chamber (95% N_2; 5% CO_2) with a culture medium lacking glucose for 12 h. The post-nuclear (PN) and nuclear fractions (N) of SK-N-SH cells after MNNG or OGD treatment were prepared, followed by immunoprecipitation of SIRT1 and immunodetection of SIRT1 and AIF as indicated. α-tubulin (the post-nuclear marker) and histone H3 (the nuclear marker) were used to control the quality of fractionation. **D** SIRT1 physically binds to AIF. Bacterially purified GST or GST-SIRT1 was incubated with His-AIF isolated from *E. coli*, and the GST pull-down assays were performed, followed by anti-GST and anti-His western blotting analysis. **E** SIRT1 deacetylase catalytic domain interacts with AIF. The schematic diagrams of SIRT1 full-length (FL) and its deletion mutants are shown in the upper panel. The indicated SIRT1 full-length plasmid and its deletion mutant plasmids were co-transfected with AIF-HA in 293 T cells, followed by anti-Flag immunoprecipitation and subsequent anti-HA western blotting analysis (lower panel). **F** The NADH and FAD domain of AIF binds to SIRT1. The schematic diagrams of AIF full-length and its deletion mutants are shown in the upper panel. The indicated vector and AIF plasmids were co-transfected with HA-SIRT1 in 293 T cells, and anti-Flag immunoprecipitation was performed followed by anti-HA western blotting (lower panel). The input of HA-SIRT1 is shown in the bottom panel.

It has been well established that AIF serves as an executioner of programmed necrosis under various necrotic stresses, and its nuclear translocation leads to irreversible chromatinolysis and necrotic cell death. Since AIF-K295 is highly conserved among species (Fig. 4D) and is acetylated in response to MNNG and OGD treatments (Fig. 4F), we hypothesized that AIF acetylation at K295 may affect AIF-mediated cell death. To test this hypothesis, we generated cell lines with AIF knockdown (AIF-shR) and subsequently established cell lines with stable re-complementation of AIF-WT and the AIF-K295R or AIF-K295Q mutants. Stable cell lines subjected to MNNG treatment were evaluated for cell viability utilizing the CCK-8 assay. The findings demonstrated that, in comparison to control cells (shN), AIF knockdown significantly increased cell viability. In contrast, complementation with AIF-WT or AIF-K295Q, but not AIF-K295R, resulted in a reduction of cell viability following MNNG exposure (Fig. 4G). Furthermore, FACS analysis revealed that complementation with AIF-WT or AIF-K295Q, unlike AIF-K295R, reinstated cell death in the context of AIF knockdown (Fig. 4H, I). The above data suggest that AIF acetylation at K295 essential for AIF-mediated cell death. Given that nuclear condensation and large-scale DNA fragmentation (~50 kb) are the most discernible phenotypes associated with AIF function in the nucleus[13], we subsequently investigate whether acetylation of AIF at K295 could modulate these processes under stress conditions. The results of the fluorescence microscopy assay showed that AIF knockdown decreased MNNG-induced nuclear condensation, and re-complementation of AIF-WT or AIF-K295Q (but not AIF-K295R) led to nuclear condensation (Fig. 4J, K). Pulsed-field gel electrophoresis analysis demonstrated that re-complementation with AIF-WT or AIF-K295Q (but not AIF-K295R) restored MNNG-induced large-scale DNA fragmentation (~50 kb) under MNNG treatment (Fig. 4L). Taken together, our results indicate that AIF-K295^{ac} is required for AIF-mediated caspase-independent chromatinolysis and programmed necrosis, and SIRT1 plays a key role in deacetylating stress-induced AIF-K295^{ac}.

SIRT1 blocks AIF-CypA interaction via AIF-K295 deacetylation

Upon necrotic stresses, AIF associates with CypA in the cytosol and migrates into the nucleus, where it cooperates with γH2AX to trigger DNA degradation and nuclear condensation[10,30,33,49]. The suppression of CypA by siRNA or the abrogation of the AIF-CypA interaction by synthetic peptides could inhibit AIF-mediated chromatinolysis and cell death[10,30,33,49]. Since AIF-K295 is located near the CypA binding domain of the AIF protein (Fig. 5A), we next examined whether AIF acetylation is required for stress-induced AIF-CypA interaction. The results showed that the AIF-K295R mutant exhibits a reduction in its association with CypA compared to AIF-WT under MNNG or OGD treatment (Fig. 5B, C). In addition, we performed an in vitro GST pull-down assay and observed that the acetylation-mimic mutant AIF-K295Q interacted with CypA with higher efficiency than either AIF-WT or AIF-K295R (Fig. 5D). These results support the idea that AIF-K295 acetylation facilitates the binding of AIF to CypA. We also examined whether SIRT1 inhibits the association between AIF and CypA under stress conditions. The results showed that overexpression of wild-type SIRT1, but not of a catalytic-deficient mutant of SIRT1 (SIRT1-H363A), markedly reduced the AIF-CypA binding under MNNG or OGD treatment (Fig. 5E). Moreover, knockdown of SIRT1 significantly increases MNNG-induced endogenous AIF-CypA binding (Fig. 5F). These data suggest that the deacetylase activity of SIRT1 is crucial for inhibiting AIF-CypA association.

A prior study demonstrated that the AIF-CypA interaction is essential for the nuclear translocation of AIF[30]. We next explored the impact of AIF-K295 acetylation on its nuclear translocation. Results of the immunofluorescence assay and mitochondrial separation experiments showed that both AIF-WT (wild-type) and AIF-K295 mutants (K295R, K295Q) localize in the mitochondria under normal culture conditions, and MNNG treatment led to a significant nuclear distribution of AIF-WT and AIF-K295Q, whereas a substantial portion of AIF-K295R was observed in the cytoplasm (Fig. 5G, H). These findings suggest that acetylation at AIF-K295 is required for the MNNG-induced translocation of AIF from the cytoplasm to the nucleus.

Previous research has demonstrated that AIF plays a crucial role in mediating programmed necrosis by forming a DNA degradation complex with CypA and γH2AX in the nucleus[28]. To further elucidate the role of SIRT1 in regulating the AIF-mediated programmed necrosis, we investigated whether SIRT1 could inhibit the formation of the DNA degradation complex. Results showed that overexpression of wild-type SIRT1 (WT), but not the SIRT1-H363A mutant, resulted in a reduction of the AIF/γH2AX/CypA complex formation under conditions of MNNG treatment (Fig. 5I). We also conducted an immunostaining assay to examine the co-localization of wild-type AIF or AIF-K295R with γH2AX and CypA following MNNG treatment. Results showed that MNNG treatment induced CypA/AIF/γH2AX complex formation in the nucleus, whereas expression of the AIF-K295R mutant resulted in reduced formation of this complex (Fig. 5J). This conclusion was further confirmed by co-immunoprecipitation analysis (Fig. 5K). Collectively, the results support that SIRT1 blocks the nuclear AIF/CypA/γH2AX complex formation under stress conditions through deacetylation of AIF-K295.

SRT1720 suppresses AIF-mediated chromatinolysis and necrotic brain injury

Previous research indicated that AIF-mediated programmed necrosis plays a crucial role in neuronal cell death after middle cerebral artery occlusion[5,50,51]. Thus, we next investigated the protective function of the SIRT1 activator SRT1720 in preventing necrotic brain injury. Prior to this investigation, we assessed the ability of SRT1720 to prevent AIF-mediated cell death in SK-N-SH neuroblastoma cell lines. The results indicated that SRT1720 led to a reduction in the percentage of TUNEL-positive cells (Fig. 6A, B) and PI/Annexin V double-positive cells (Fig. 6C, D). This effect was associated with decreased levels of AIF-K295^{ac} (Fig. 6E). Furthermore, activation of SIRT1 by SRT1720 resulted in a significant increase in cell viability following MNNG treatment (Fig. 6F). Next, we evaluated whether the pharmacological activation of SIRT1 by SRT1720 inhibits programmed necrosis in vivo. A previous study reported that occlusion for >3 h could cause severe ischemic

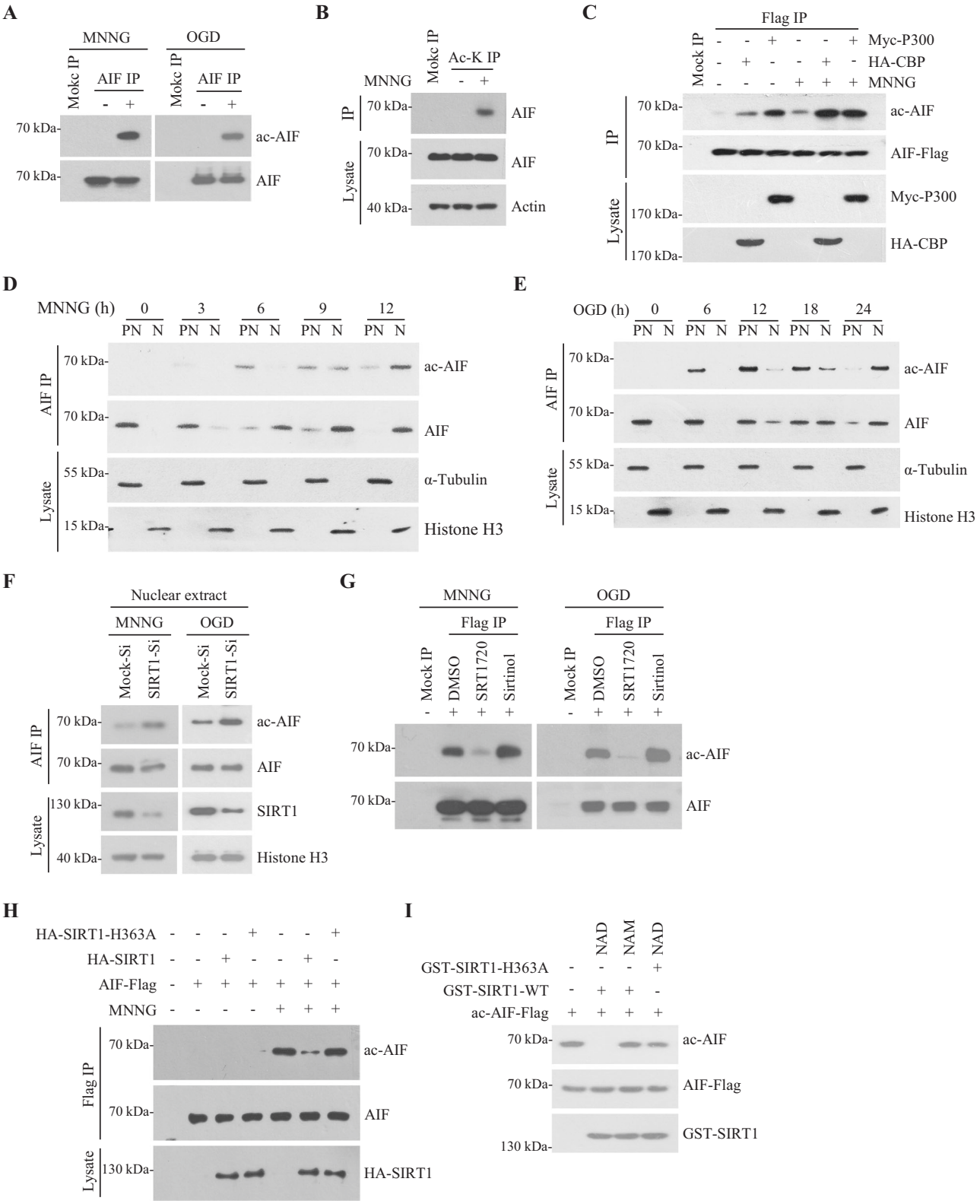

lesions[38,39]. In this study, mice were pre-treated with vehicle or SRT1720 for 12 h and then subjected to 4 h of MCAO treatment. Results showed that, relative to vehicle-treated mice, mice pre-treated with SRT1720 showed a marked decrease in both the volume of cerebral infarct and the level of large-DNA fragmentation under MCAO (Fig. 6G-H). Consistently, a reduction in AIF-K295^{ac} was observed in SRT1720 pre-treated mice (Fig. 6I), and SRT1720 treatment affects the distribution of AIF between nuclear and post-nuclear (Fig. 6J). In brains of mice model, although SIRT1 localizes to nucleus primarily, it shows nucleus and cytoplasmic localization after MCAO treatment, which was first reported by Jesús M. Pradillo group[52]. Therefore, our data also support the idea that, in brain cells, SRT1720 may increase cytoplasmic SIRT1 activity to deacetylate AIF-K295^{ac}, thereby limiting AIF nuclear translocation in vivo. These results suggest that pharmacological activation of

Fig. 3 | SIRT1 deacetylates AIF. A SK-N-SH cells were harvested 12 h after MNNG or OGD treatment. For MNNG treatment, cells were incubated with a culture medium containing 500 μM MNNG for 20 min, then re-cultured for another 12 h in fresh medium. The whole-cell lysates were then prepared and immunoprecipitated with anti-AIF antibody and blotted with anti-acetylated lysine antibody as indicated. The acetylation of AIF was analyzed by western blot. **B** SK-N-SH cells were harvested 12 h after MNNG treatment, then the whole-cell lysates were prepared and immunoprecipitated with anti-acetylation antibody (Ac-K IP) as indicated. The acetylation status of AIF following MNNG treatment was analyzed by western blot using anti-AIF antibody. **C** 293 T cells were transiently transfected with AIF-Flag, HA-CBP, or Myc-p300 plasmids for 24 h, cells were harvested 12 h after MNNG treatment, then cell lysates were immunoprecipitated with FlAG-M2 beads, followed by western blotting with anti-acetylated lysine, anti-HA, and anti-Myc antibodies. **D**-**E** SK-N-SH cells were harvested at the indicated times after MNNG or OGD treatment. The post-nuclear and nuclear extracts from the cells were immunoprecipitated with an anti-AIF antibody and analyzed by western blotting with anti-acetylated lysine and anti-AIF antibodies, respectively. Histone H3 (nuclear marker) and α-tubulin (post-nuclear marker) were used to control for fraction quality and protein loading. **F** Scramble siRNA (Mock-si) or siRNA against human SIRT1 (SIRT1-si) was transfected into SK-N-SH cells. About 48 h after transfection, cells were treated with MNNG or OGD for another 12 h. Then, cells were harvest and nuclear extracts were immunoprecipitated with an anti-AIF antibody, and acetylated AIF in the nucleus was detected (upper panel). SIRT1 expression was examined by western blotting (lower panel). **G** 293 T cells were transfected with either a vector or AIF-Flag plasmids were pre-treated with DMSO, SRT1720 (10 μM) or Sirtinol (50 μM) for 12 h followed by 20 min of treatment with 500 μM MNNG. The cells were then maintained in fresh medium for another 12 h. Cell lysates were immunoprecipitated with Flag-M2 beads, followed by western blotting with an anti-acetylated lysine antibody. **H** 293 T cells co-transfected with indicated plasmids were treated with 500 μM MNNG for 20 min, then the cells were maintained in fresh medium for another 12 h. Cells were lysed and immunoprecipitated with FLAG-M2 beads, followed by western blot analysis. AIF acetylation (ac-AIF) was detected using anti-acetylated lysine or anti-Flag antibodies. **I** In vitro deacetylation of AIF by SIRT1. Purified AIF from 293 T cells was incubated with recombinant *E. coli*-expressed GST-SIRT1 wild-type (WT) or GST-SIRT1-H363A protein in the absence or presence of nicotinamide adenine dinucleotide (NAD) (50 mM) or NAM (200 mM) for 2 h at 30 °C. The ac-AIF level was detected using an anti-acetylated lysine antibody.

SIRT1 could be a potential clinical strategy against necrotic stimuli-induced chromatinolysis and brain injury.

Based on the findings of this study and existing literature[7,10,11,35,42,44,53,54], we present a theoretical framework for the role of AIF acetylation and SIRT1 in regulating AIF-dependent chromatinolysis and programmed necrosis. Under normal circumstances, AIF is localized in the mitochondria. However, in response to necrotic stimuli (such as MNNG, OGD, hypoxia-ischemia), AIF is released from the mitochondria, then AIF undergoes acetylation at K295 (AIF-K295^{ac}) within the cytosol and thus interacts with CypA to aid in its translocation to the nucleus. Given SIRT1 is present not only in the nucleus but also in the cytoplasm in brain cells[52], therefore SIRT1 may use two pathways to restrict AIF-mediated necrotic chromatinolysis in the brain: the cytoplasmic SIRT1 inhibits AIF cytoplasm-to-nucleus translocation by deacetylating AIF-K295^{ac}, the nuclear SIRT1 deacetylates AIF-K295^{ac} to hinder the assembly of the AIF/CypA/γH2AX chromatinolysis complex, ultimately inhibiting AIF-mediated caspase-independent chromatinolysis and programmed necrosis (Fig. 6K).

Discussion

The complexity and abundance of initiation and propagation factors present challenges in pinpointing optimal drug targets for programmed necrosis[1]. Previous studies have demonstrated that upon activation of PARP-1, AIF is released into the cytosol, subsequently translocating to the nucleus and triggering irreversible chromatinolysis, which leads to necrotic cell death[13,28]. Consequently, prior investigations have primarily concentrated on inhibiting the sequential activation of PARP-1, calpains, Bid, and BAX, as well as the liberation of AIF from the mitochondria[42]. PARP-1 helps maintain cellular balance and genetic integrity by repairing DNA damage through base-excision repair. Excessive activation of PARP-1 can lead to the release of AIF from the mitochondrion[43]. The translocation of AIF from the mitochondria to the nucleus results in chromatin condensation and DNA fragmentation, leading to necrotic cell death. Thus, PARP-1 inhibitors may be effective in treating diseases related to the overactivation of PARP-1[5]. However, the long-term use of PARP-1 inhibitors may give rise to adverse effects due to the inhibition of PARP-1 activity, which is essential for maintaining genomic stability[5]. Our study found that necrotic stress leads to the production of AIF-K295^{ac}, which then associates with CypA and translocates into the nucleus. Moreover, SIRT1 inhibits AIF-mediated programmed necrosis by deacetylating AIF-K295^{ac} in the nucleus. The SIRT1 activator SRT1720 reduces necrotic brain injury by lowering AIF-K295^{ac} levels. These results support the idea that AIF-mediated programmed necrosis can be regulated by acetylation and deacetylation modifications. Additionally, AIF-mediated caspase-independent chromatinolysis and programmed necrosis can be switched off in the nucleus. This indicates that directly targeting of the execution stage of necrosis is a promising approach for the treatment of necrosis-related diseases.

Previous studies have identified the major components of the caspase-independent chromatin DNA degradation complex, including AIF, CypA[33], MIF[34] and γH2AX[10]. However, the regulatory mechanisms inhibiting AIF-mediated DNA degradation remain unclear. Previous research has demonstrated the necessity of the AIF-CypA interaction for AIF nuclear translocation[30] and chromatinolysis[33]. Recent studies have demonstrated the molecular assembly of AIF/CypA/γH2AX and the collaborative interactions among its protein constituents in the degradation of genomic DNA into large-scale fragments[54]. Our results showed that acetylation of AIF-K295 functions as a critical posttranslational modification mechanism that enhances stress-induced AIF-CypA interaction. The deacetylation of AIF-K295^{ac} by SIRT1 hinders AIF nuclear translocation and chromatinolysis under necrotic stress conditions, indicating that precise control of AIF-K295^{ac} is vital for AIF-mediated programmed necrosis. Notably, it has been observed that macrophage migration inhibitory factor (MIF) plays a role in AIF-mediated chromatinolysis in mammalian cells[34]. Biochemical analyses have revealed that CypA and MIF display distinct preferences for DNA cleavage[34,55], suggesting a potential collaborative contribution to AIF-mediated chromatinolysis. Recent research has also highlighted that the deacetylation of MIF at K78 by histone deacetylase HDAC6 disrupts its interaction with AIF, and HDAC6 regulates brain injury following ischemic stroke[56]. Thus, it is attractive to further study the role of protein posttranslational modifications in regulating AIF-associated proteins and their roles in mediating chromatinolysis and necrotic cell death.

SIRT1 has protective effects in a range of pathological conditions, including cardiovascular diseases, neurodegeneration, inflammation, metabolic diseases, and aging-related conditions[18]. The neuroprotective functions of SIRT1 in cerebral ischemia has been extensively documented, primarily through its modulation of various downstream pathways such as mitochondrial function, antioxidation, DNA repair, synaptic function, blood flow regulation, and neuroinflammation[57]. Moreover, the nuclear translocation of AIF has been documented in numerous pathological conditions linked to neurodegeneration, including Alzheimer's disease[58] and Parkinson's disease brain samples[59], neuronal cells expressing expanded polyglutamine repeats in Huntingtin proteins[60], and motor neurons of

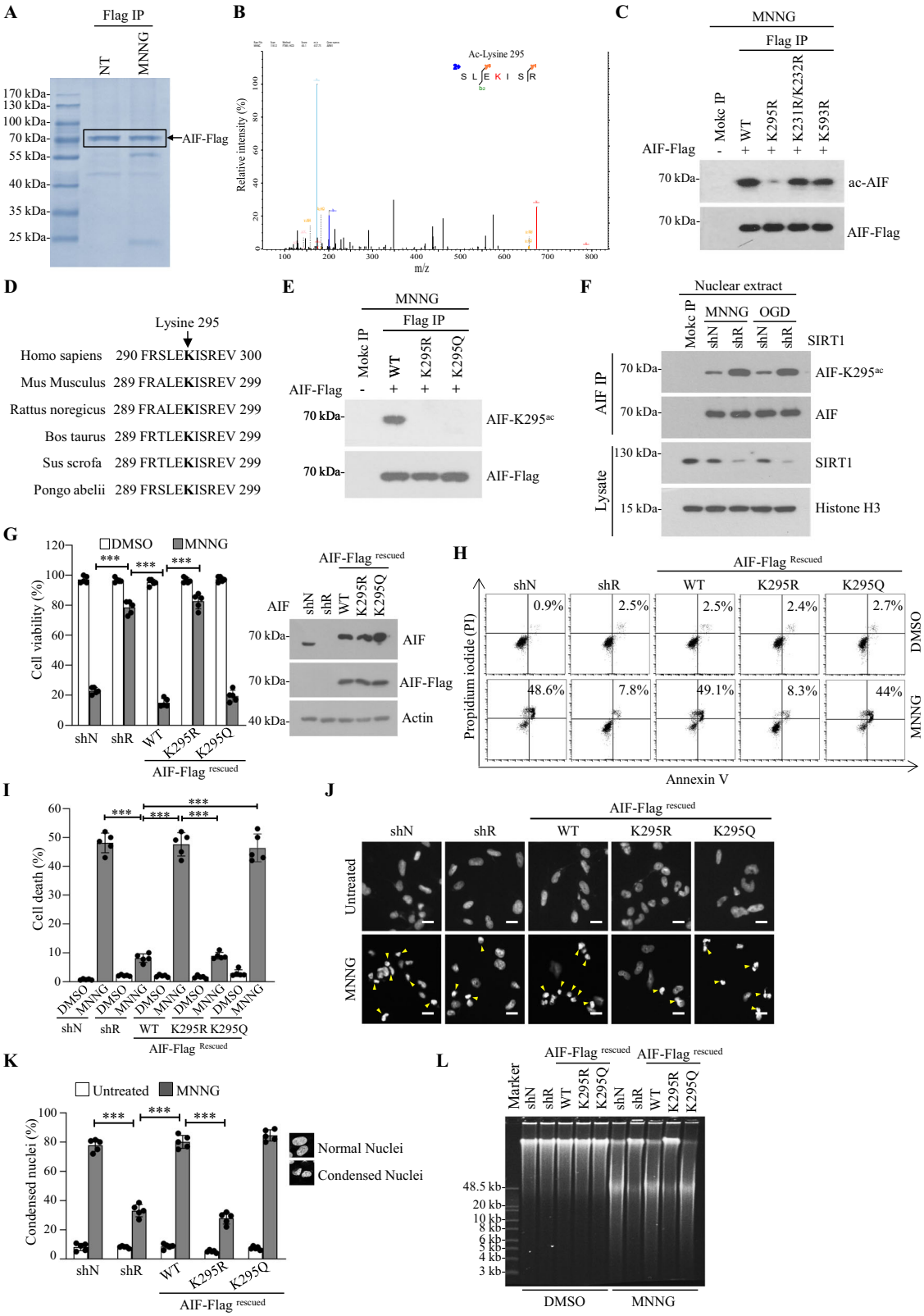

symptomatic SOD1-G93A transgenic mice[61]. These studies suggest a role for AIF-mediated cell death in chronic neuropathology. Our study elucidated a function of SIRT1 as a safeguard against necrotic stimuli-induced brain injury by suppressing AIF-mediated caspase-independent chromatinolysis within the nucleus, and SRT1720 markedly blocked MCAO-induced necrosis and brain injury. We suggest that pharmacological activation of SIRT1 may also be benefit for chronic neuropathology diseases. Further study of the activity of the pharmacological SIRT1 allosteric activators such as STAC-5 and STAC-8[62] in regulating caspase-independent chromatinolysis and programmed necrosis may bring more advancements in the treatment of diseases associated with necrosis.

Fig. 4 | AIF-K295 acetylation is required for chromatinolysis and programmed necrosis. A Representative SDS-PAGE and Coomassie blue staining of Flag-immunoprecipitants (Flag IP) obtained from AIF-Flag overexpressing 293 T cells untreated (NT) or treated with MNNG for 20 min and then replaced with fresh medium for 12 h. The purified AIF-Flag (indicated by the square) samples were cut from the SDS-PAGE gel and submitted for mass spectrometry analysis. **B** AIF acetylation was analyzed by mass spectrometry, and the acetylation of AIF lysine 295 was detected in the MNNG-treated sample. **C** 293 T cells transfected with the indicated AIF-Flag or its mutant plasmids were lysed and immunoprecipitated using FLAG-M2 beads, followed by western blotting with an anti-acetylated lysine antibody. Total AIF was detected using an anti-AIF antibody. **D** Sequence alignment of the region containing the acetylation site in AIF from different species. The schematic diagram shows that lysine 295 of AIF is highly conserved across multiple species. **E** 293 T cells transfected with the indicated wild-type AIF-Flag or AIF-K295R, AIF-K295Q as indicated. 24 h after transfection, cells were treated with MNNG for 20 min and then replaced with fresh medium for another 12 h. Then, the cell lysates were immunoprecipitated using FLAG-M2 beads and blotted with an anti-AIF-K295^{ac} antibody. **F** Control shRNA (shN) or SIRT1-specific shRNA stable-expressing (shR) SK-N-SH cells were treated with MNNG or OGD. For MNNG treatment, cells were treated with 500 μM MNNG for 20 min, then cells were maintained in fresh medium for another 12 h. For OGD treatment, cells were placed in an I-CONIC hypoxic chamber (95% N_2; 5% CO_2) with a culture medium lacking glucose for 12 h. Subsequently, cells were lysed, and the nuclear fractions were immunoprecipitated using an anti-AIF antibody, followed by AIF-K295^{ac} blotting. **G** Control shRNA (shN) or AIF-specific shRNA stable-expressing (shR), AIF-specific shRNA stable-expressing (shR) rescued with AIF-Flag (WT, K295R, or K295Q) SK-H-SH cells, were treated with DMSO or 500 μM MNNG for 20 min, then, cells were maintained in fresh medium for another 2 days. A CCK-8 assay was performed to measure cell survival rate. The data represent the means of five independent experiments ($n = 5$) ± SD and are shown in each column. ***$p < 0.01$ (left panel). The AIF expression was examined by western blot using anti-AIF and anti-Flag antibodies, actin was used as a loading control (right panel). **H**, **I** Control shRNA (shN) or AIF-specific shRNA stable-expressing (shR), AIF-specific shRNA stable-expressing (shR) rescued with Flag-AIF (WT, K295R, or K295Q) SK-N-SH cells were treated with DMSO or 500 μM MNNG for 20 min, then cells were maintained in fresh medium. 4 h after MNNG treatment, cells were labeled with Annexin V-FITC and PI and analyzed by flow cytometry. Representative cytofluorometric plots are shown (**H**), and the frequency of Annexin V and PI positive labeling was recorded and expressed as a plot (**I**). The data represent the means of five independent experiments ($n = 5$) ± SD and are shown in each column. ***$p < 0.01$. **J**, **K** Control shRNA (shN) or AIF-specific shRNA stable-expressing (shR), and AIF knockdown (shR) rescued with AIF-Flag (WT, K295R, K295Q) SK-N-SH cells were untreated or exposed to 500 μM MNNG for 20 min. Subsequently, the cells were incubated in fresh medium for an additional 12 h. Following this, the cells were stained with DAPI and examined using fluorescence microscopy, with a scale bar indicating 10 μm. Condensed nuclei were identified with yellow arrows (**J**). Statistical analysis of the condensed nuclei was conducted as described (**K**). The data represent the means of five independent experiments ($n = 5$) ± standard deviation (SD) and are presented in each column. Statistical significance was determined at ***$p < 0.01$. **L** Control shRNA (shN), AIF-specific shRNA stable-expressing (shR), and AIF-specific shRNA stable-expressing (shR) rescued with AIF-Flag (WT, K295R, K295Q) SK-N-SH cells treated with DMSO or 500 μM MNNG for 20 min. The cells were then maintained in fresh medium for another 8 h and subjected to nuclear DNA extraction and pulsed-gel electrophoresis to visualize DNA fragments (~50 kb).

Materials and methods

Cell Lines, plasmids, and reagents

HEK293T and SK-N-SH cell lines were obtained from Cell Bank/Stem Cell Bank of Chinese Academy of Sciences. The AIF knockdown plasmid was generated by inserting the sequence: CGGCCCACAGTGGAATTGGCAAACCTCGAGGTTTGCCAATTCCACTGTGGGTTTTTG, which contains the 3' UTR region of AIF (underlined), into the AgeI and EcoRI restriction sites of pLKO.1. The SIRT1 knockdown plasmid was generated by inserting the sequence: CCGGGTTGGATGATATGACACTGCTCGAGCAGTGTCATATCATCCAACTTTTTG, which contains the CDS region of SIRT1 (underlined), into the AgeI and EcoRI restriction sites of pLKO.1. This sequence has already been verified and used in our previous publication[20]. Stable knockdown or control cell lines were established by lentivirus infection and selected with puromycin. The expression plasmids of HA-SIRT1, Flag-SIRT1, and Flag-SIRT1 deletions were described in our previous publications. The expression plasmids of C-terminal Flag, HA, and His-tagged AIF were generated by PCR using cDNA obtained from 293T cells as a template, along with two primers: AIF forward (5'-GGAATTCATGTTCCGGTGTGGAGGCCT-3'), which contains an EcoRI site (underlined), and AIF reverse (5'-ATTTGCGGCCGCACAGTCTTCATGAATGTTGAATAGT-3'), which contains a NotI site (underlined). A lentiviral-based AIF expression plasmid was constructed by inserting an AIF cDNA fragment into the SmaI restriction site of a lentiviral empty vector. The AIF cDNA fragment was produced by PCR using a full-length AIF-Flag plasmid described above as the template, along with two primers: AIF forward: 5'-TCCCCCGGGACTAGTCCAGTGTGGTGGAATT-3', which contains the SmaI site (underlined), and AIF reverse: 5'-TCCCCCGGGAACAGATGGCTGGCAACTAG-3', which also contains the SmaI site (underlined). The AIF site mutants K231R/K232R, K295R, K593R, and K295Q plasmids were generated using wild-type AIF-Flag as a template via PCR. The primers for these constructions are as follows: K231R/K232R forward: 5'-GGCTGTCCTCACTGGGAGGAGGGTAGTACAGCTGG-3'; K231R/K232R reverse: 5'-CAGCTGTACTACCCTCCTCCCAGTGAGGACAGCC-3'; K295R forward: 5'-GACTTTAGAAGCTTGGAGAGGATTTCACGGGAAGTCAAA-3'; K295R reverse: 5'-TTTGACTTCCCGTGAAATCCTCTCCAAGCTTCTAAAGTC-3'; K295Q forward: 5'-ACTTCCCGTGAAATCTGCTCCAAGCTTCTAAAGTCTC-3'; K295Q reverse: 5'-ACTTTAGAAGCTTGGAGCAGATTTCACGGGAAGTCA-3'; K593R forward :5'-TGCTCACCGTCCCTAATGATCTTCCTTGCTATTGGC-3'; K593R reverse: 5'-GCCAATAGCAAGGAAGATCATTAGGGACGGTGAGCA-3'. The siRNA against SIRT1 (5'-GUUGGAUGAUAUGACACUGtt-3'), siRNA against AIF (5'-CACGUGGAAUUGGCAAACtt-3'), and control siRNA (5'-UUCUCCGAACGUGUCACGUtt-3') were synthesized by Shanghai GenePharma. Double-stranded siRNA was transiently transfected into cells using Lipofectamine 3000 (Invitrogen). anti-Flag M2 Affinity Agarose Gel, anti-HA Agarose, Flag peptide, HA peptide, Thiazolyl Blue Tetrazolium Blue (MTT), and TTC (2,3,5-Triphenyl-tetrazolium chloride solution) were purchased from Sigma. Cell Counting Kit-8 (C0038), Anti-Fade Mounting Medium (P0126), one-step TUNEL assay kit (C1090), and Cell Mitochondria Isolation Kit (C3601) were obtained from Beyotime Biotechnology. The Plasmid Prep Kit (DP103) and DNA Purification Kit (DP204) were purchased from TIANGEN BIOTECH Co., Ltd. The FITC Annexin V/PI detection kit (556547) was obtained from BD Biosciences. ECL western blotting Substrates (32106), Lipofectamine 3000 (L3000001), Goat anti-Mouse Secondary Antibody conjugated with Alexa Fluor™ 488, Goat anti-Rabbit Secondary Antibody with Alexa Fluor™ 568, Goat anti-Mouse Secondary Antibody with Alexa Fluor™ 633, and DNA restriction enzymes were obtained from Thermo Fisher Scientific. The anti-CypA antibody (ab41684) was obtained from Abcam. The anti-SIRT1 (H-300) antibody, anti-Histone 3 (FL-136) antibody, anti-AIF (E-1) (sc-13116) antibody, and Protein A/G PLUS-Agarose (sc-2003) were purchased from Santa. Anti-Acetylated-lysine (Ac-K^2-100) MultiMab™ Rabbit mAb, acetylated-lysine Mouse mAb (Ac-K-103), and anti-HA-tag (C29F4) rabbit mAb were obtained from Cell Signaling Technology. anti-AIF (A2568), anti-SIRT1 (A19667) rabbit mAb, anti-Flag rabbit mAb (AE092), anti-PARP-1 (A0942) rabbit mAb, and anti-MIF (A1391) rabbit mAb were obtained from ABclonal.

Cell culture and cell death induction

SK-N-SH cells were cultured in MEM Alpha Basic medium (Gibco) supplemented with 10% FBS, 1 mM Sodium Pyruvate, MEM NEAA, GlutaMAX, and 100 U/ml penicillin/streptomycin (Sangon Biotech). HEK293T was cultured in DMEM supplemented with 10% FBS and 100 U/ml penicillin/streptomycin (Sangon Biotech), and maintained at 37 °C in a 5% CO_2 atmosphere. To induce cell death and AIF release, cells were treated with MNNG or OGD (oxygen-glucose deprivation). The MNNG experiments were carried out as described previously[10]. In detail, the SK-N-SH and HEK293T cells were maintained in culture medium with MNNG (500 μM)

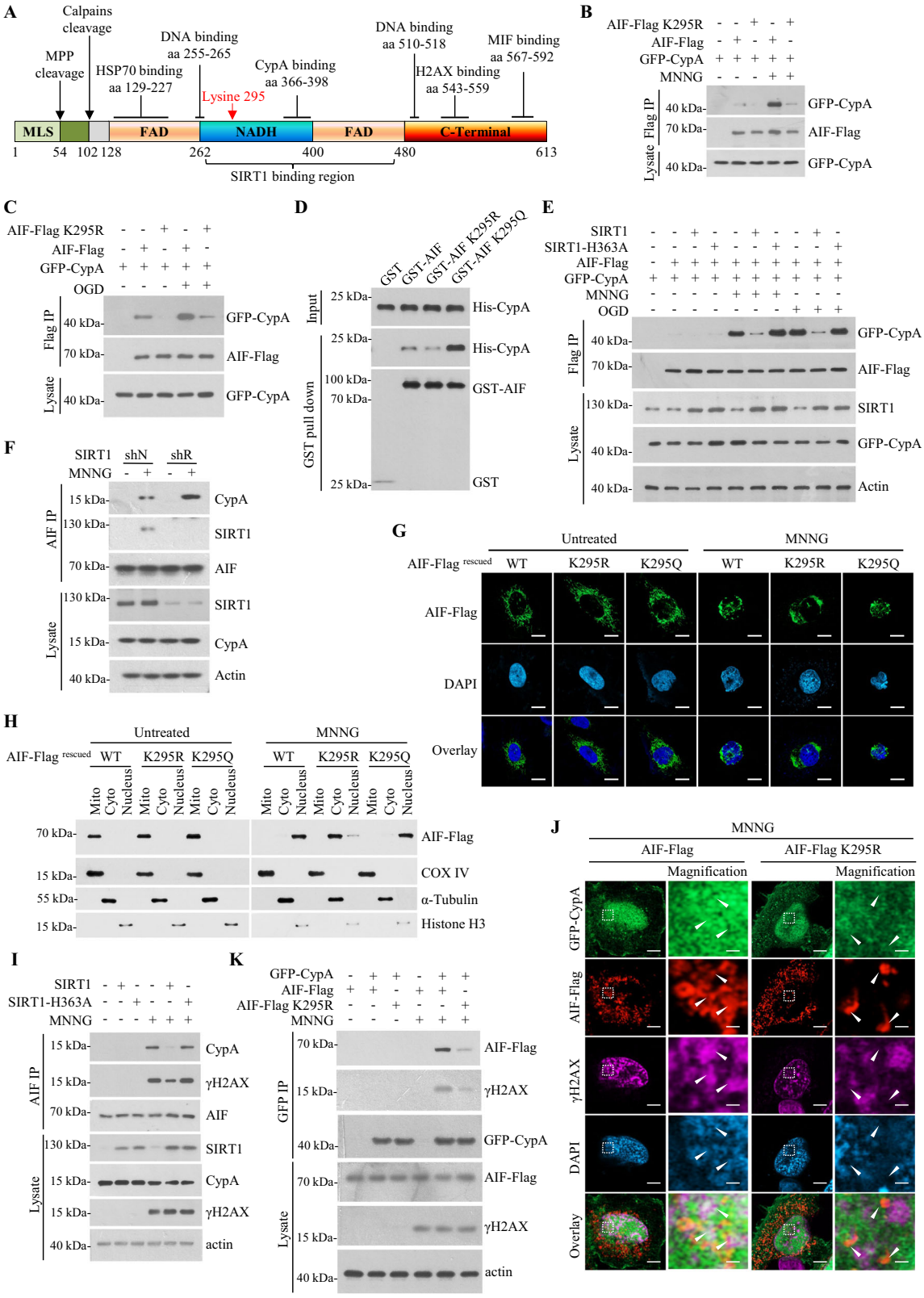

for 20 min before the culture medium was removed. Following this, the cells were washed with PBS three times and cultured in fresh medium without MNNG for the indicated time periods. OGD was carried out after the SK-N-SH cells had been seeded for 24 h. The cells were placed in an I-CONIC hypoxic chamber (Baker Ruskinn) after the culture medium was replaced with oxygen-glucose-free medium. The chamber was then sealed and flushed with a mixture of 95% N_2 and 5% CO_2. Finally, the chamber was set to 37 °C for the indicated duration of OGD.

Acetylation specific antibodies

Rabbit antiserum against AIF acetylation at K295 was raised using the peptide (CRDPSLRK[Ac]SGV), where K295 is acetylated and indicated as

Fig. 5 | SIRT1 inhibits the AIF-CypA complex formation through deacetylating AIF-K295. A The schematic representation of AIF illustrates its structural domains and binding motifs. The full-length AIF comprises a Mitochondrial Localization Sequence (MLS, depicted in green), a putative Transmembrane Domain (TM, also in green), a flavin adenine dinucleotide (FAD)-bipartite domain (colored orange), an NADH-binding motif (blue), and a C-terminal domain (red). The TM is bordered by two proteolytic cleavage sites: a mitochondrial processing peptidase (MPP) cleavage site at residue 54 and a calpain/cathepsin cleavage site at residue 102. Various proteins, including Hsp70, Cyclophilin A (CypA), phosphorylated H2AX (γH2AX), and Macrophage Migration Inhibitory Factor (MIF), interact with AIF at distinct regions. The numerical annotations correspond to specific amino acid positions. Additionally, the SIRT1-binding motif on AIF is located between residues 262 and 480. **B**, **C** GFP-tagged CypA was co-transfected with AIF-Flag or AIF-Flag K295R expression plasmids, followed by treatment with MNNG (12 h) or OGD (12 h). For MNNG treatment, cells were treated with 500 μM MNNG for 20 min, and then cells were maintained in fresh medium for another 12 h. Cells lysates were immunoprecipitated with FLAG-M2 beads followed by western blotting with anti-GFP and anti-AIF antibodies. **D** Binding of GST-AIF and GST-AIF-mutants to His-CypA in vitro. Bacterially purified GST, GST-AIF, and its mutants were incubated with His-CypA isolated from *E. coli*, and the GST pull-down assays were performed, followed by anti-GST and anti-His western blotting analysis. **E** 293 T cells co-transfected with the indicated plasmids were treated with or without MNNG (12 h) or OGD (12 h). The cells were then lysed and immunoprecipitated with FLAG-M2 beads, and the co-precipitated CypA was blotted for GFP antibody. **F** Control shRNA (shN) and SIRT1-specific shRNA stable-expressing (shR) SK-N-SH cells were treated with 500 μM MNNG for 20 min. The cells were maintained in fresh medium for another 12 h. After that, the cells were lysed and immunoprecipitated using an anti-AIF antibody (AIF IP), and co-precipitated proteins were blotted with anti-CypA and anti-SIRT1 antibodies (upper panel). CypA and SIRT1 expression levels were examined by western blot (lower panel). **G** SK-N-SH AIF stable knockdown (shR) cells rescued with Flag-AIF (WT, K295R/Q) were treated with or without MNNG as indicated. For MNNG treatment, cells were treated with 500 μM MNNG for 20 min, after which they were maintained in fresh medium for another 12 h. Subsequently, the cells were co-stained with anti-Flag antibody (green), DAPI (blue), and visualized using a fluorescence microscope (scale bars indicate 10 μm). **H** SK-N-SH AIF stable knockdown (shR) cells rescued with Flag-AIF (WT, K295R/Q) used in (**G**) were treated with or without MNNG as described above. The mitochondrial, cytosolic, and nuclear extracts were analyzed by western blotting for the presence of AIF. COX IV (mitochondrial marker), α-tubulin (cytosolic marker) and histone H3 (the nuclear marker) were used to control fractionation quality and protein loading. **I** SK-N-SH cells were transfected with either SIRT1 or the SIRT1-H363A mutant, as specified. Subsequently, cells were treated with 500 μM MNNG for 20 min, then cells were maintained in fresh medium for another 9 h. Following treatment, cell lysates were prepared and subjected to immunoprecipitation using an AIF antibody. The co-precipitated proteins, CypA and γH2AX, were analyzed by western blot. **J** SK-N-SH cells were transfected with GFP-CypA, AIF-Flag, and AIF-Flag K295R, as indicated. Cells were treated with 500 μM MNNG for 20 min, then cells were maintained in fresh medium for another 9 h, after which they were fixed and stained for Flag (red), GFP-CypA (green), and γH2AX (magenta). Confocal fluorescence microscopy was employed to visualize the stained cells. The nuclei were counterstained with DAPI (blue). Scale bars indicate 2 μm. Magnification scale bars indicate 0.25 μm. **K** SK-N-SH cells were transfected with GFP-CypA, AIF-Flag, and AIF-Flag K295R, as specified. Cells were treated with 500 μM MNNG for 20 min, then cells were maintained in fresh medium for another 9 h, then the cells were harvested and subjected to immunoprecipitation using GFP Magnetic Beads. The co-precipitated proteins were analyzed by western blotting with anti-Flag and anti-γH2AX antibodies (upper panel).

K[Ac]. The antiserum was pre-cleaned by affinity chromatography using the corresponding non-acetylated peptide (CRDPSLRKSGV) coupled to Sulfolink coupling resin (Thermo Scientific) and further purified by affinity chromatography using acetylated peptide (CRDPSLRK[Ac]SGV).

Flow cytometry

Cell viability was measured using an Annexin V-FITC/PI detection kit. Cell death was recorded in a BD Accuri™ C6 Flow Cytometer (BD Biosciences) for a total population of 8000 cells, with manual adjustment of color compensation based on the negative control. The detailed operational procedures can be found in the "Technical Data Sheet" accompanying the reagent kit. Data were exported using BD Accuri™ C6 software and further analyzed with FlowJo software.

Immunoprecipitation and In Vitro binding

Cell lysate preparation and protein immunoprecipitation were performed as previously described[21,22]. For the in vitro binding assay, GST-fusion and His-fusion constructs were introduced into E. coli BL21 (DE3), and the fusion proteins were induced with 0.1 mM IPTG for 8 h at 18 °C. The proteins were purified using glutathione-Sepharose 4B resin or Ni-NTA agarose beads. For the binding assay, GST or GST-SIRT1 was incubated with His-AIF in binding buffer (100 mM NaCl, 50 mM Tris-HCl pH 7.5, 15 mM EGTA, 1 mM DTT, 1 mM PMSF, 0.2% Triton X-100) for 2 h at 4 °C. The protein complex was pulled down with glutathione-agarose beads, washed, and subjected to western blot analysis.

Immunofluorescence staining

Immunofluorescence was performed as previously described[21,63]. Briefly, cells were fixed in 4% paraformaldehyde for 10 min at room temperature and washed three times with PBS. Then, cells were incubated with permeabilization buffer (0.3% Triton X-100 in PBS) for 10 min at room temperature, followed by blocking with 2% BSA. After that, cells were incubated with the primary antibody for 2 h at room temperature or overnight at 4 °C followed by incubation with fluorescently conjugated secondary antibodies (Alexa Fluor 488-tagged anti-rabbit, Alexa Fluor 594-tagged anti-mouse and Alexa Fluor 633-tagged anti-mouse secondary antibodies) for 1 h at room temperature.

Subcellular fractionation

The adherent cells were harvested and suspended in hypotonic buffer (10 mM Hepes, pH 7.9, 10 mM KCl, 0.1 mM EDTA, and 0.1 mM EGTA with protease inhibitors) and left on ice for 15 min. They were then homogenized by 15 strokes with a 1 mL needle, followed by centrifugation at 10,000 g for 1 min at 4 °C. The supernatant was retained. The nuclear extraction buffer (20 mM Hepes, pH 7.9, 0.4 M NaCl, 1 mM EDTA, 1 mM EGTA, and 1% Triton X-100 with protease inhibitors) was added to the cell pellets. The sample was left on ice for 30 min and vortexed for 3–5 s every 5 min, followed by centrifugation for 5 min at full speed (10,000 g) at 4 °C. The resultant supernatant was the nuclear fraction. Triton X-100 was added to the supernatant obtained from the first centrifugation to reach a final concentration of 1%, followed by sonication and centrifugation at 10,000 g for another 10 min. The supernatant was then considered the post-nuclear fraction. The integrity of nuclear and post-nuclear fractions was verified by detecting α-tubulin (cytoplasmic marker) and histone H3 (nuclear marker).

The Cell Mitochondria Isolation Kit was used for mitochondrial isolation. Briefly, wash the cells with PBS once. Then, digest the cells with trypsin-EDTA Solution and centrifuge at room temperature for 5–10 min to collect them. Add 1 ml of mitochondrial separation reagent to 20 million cells before use, gently suspend the cells, and let them sit in an ice bath for 10–15 min. Next, transfer the cell suspension to a glass homogenizer and homogenize for about 10–30 s. After ~20 rounds of homogenization, add 5 μl of the cell suspension to 30 μl of trypan blue staining solution. After mixing, observe the proportion of trypan blue-positive (blue) cells under a microscope. When the positive ratio exceeds 50%, the homogenization can be stopped, and the process can proceed to the next step. The mixture is then centrifuged at 600 g at 4 °C for 10 min. The nuclear fraction is found in the precipitate. After that, carefully transfer the supernatant to another centrifuge tube and centrifuge it at 11,000 g at 4 °C for 10 min. The supernatant contains the cytoplasmic proteins, while the precipitate contains the isolated cell mitochondria.

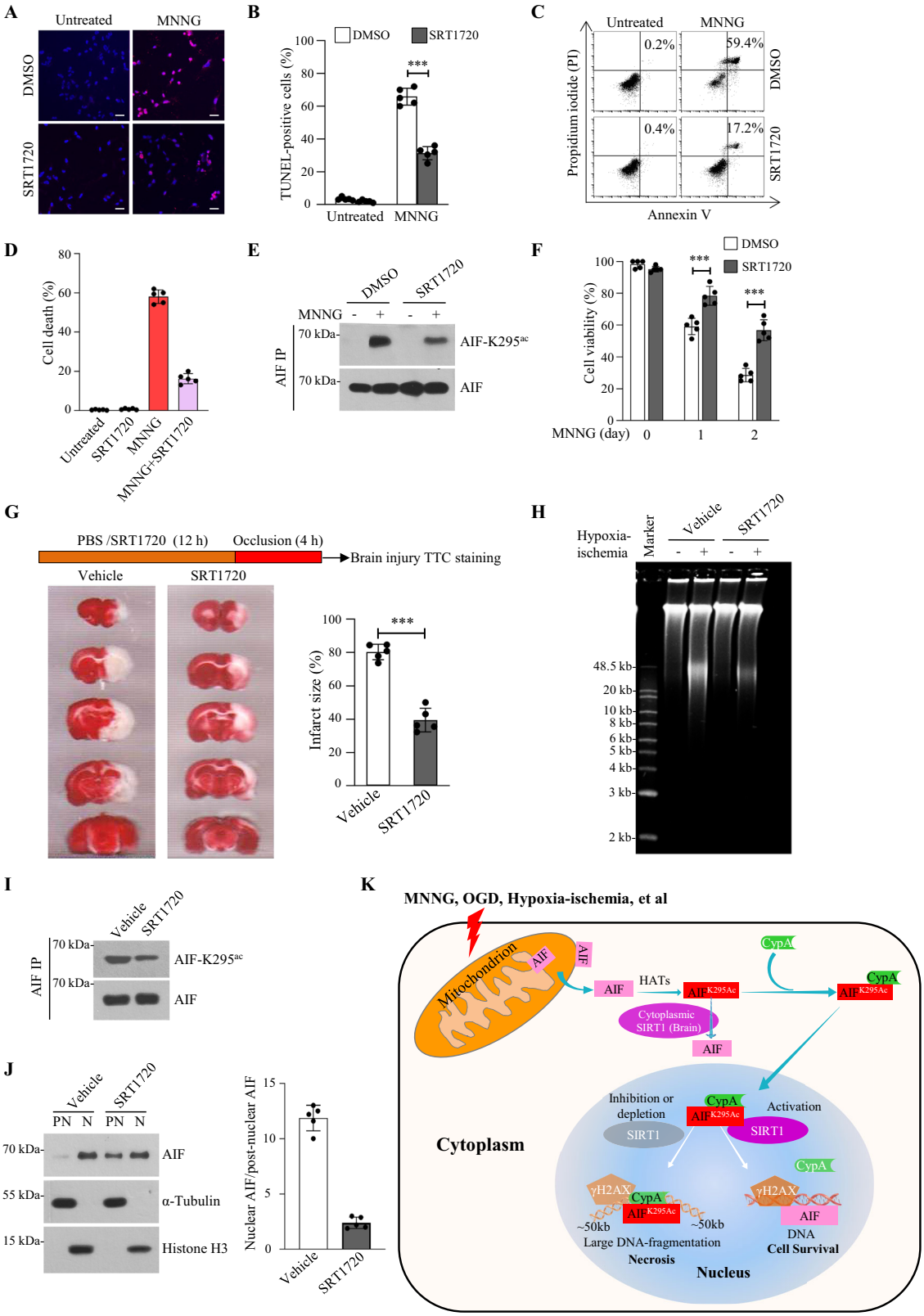

In Vitro deacetylation assay

The In vitro deacetylation assay was performed as previously described[21,64]. Briefly, 293 T cells overexpressing C-terminal Flag-tagged AIF were harvested about 12 h after MNNG treatment. The cells were then lysed and immunoprecipitated with Anti-FLAG M2 agarose (Sigma), and the enriched AIF proteins were eluted with FLAG peptide. The eluted proteins were incubated with GST-SIRT1 or GST-SIRT1-H363A in deacetylation buffer (50 mM Tris-HCl, PH 7.0, 50 mM NaCl, 10 mM $ZnCl_2$, 0.5 mM DTT, 0.1 mM PMSF, 5% glycerol, 0.02% NP-40, and protease inhibitors) in the presence or absence of 50 mM NAD^+ or 200 mM NAM for 2 h at 30 °C. The reactions were subjected to SDS-PAGE and analyzed by western blot.

Fig. 6 | SRT1720 suppresses AIF-mediated chromatinolysis and necrotic brain injury. A, **B** SK-N-SH cells were pre-treated with DMSO or SIRT1 activator SRT1720 (10 μM) for 12 h as indicated. Then, the cells were untreated or treated with MNNG and stained 3'-OH DNA breaks (TUNEL, red) and analyzed using a fluorescence microscope. DAPI (blue) was used to visualize the nuclei. For MNNG treatment, cells were treated with 500 μM MNNG for 20 min, then cells were maintained in fresh medium for another 8 h. Representative overlay pictures are shown (**A**). Scale bars indicate 20 μm. And the frequency of TUNEL-positive labeling (% cell death) in (**A**) was counted and plotted as a percentage of total cells (**B**). The data represent the means of five independent experiments ($n = 5$) ± SD and are shown in each column. ***$p < 0.01$. **C**–**E** SK-N-SH cells were pre-treated with DMSO or the SIRT1-specific activator SRT1720 at a concentration of 10 μM for 12 h. Subsequently, the cells were untreated or exposed to MNNG. Following treatment, the cells were stained with Annexin V-FITC and propidium iodide (PI) and subsequently analyzed using flow cytometry 9 h after treatment. Representative cytofluorometric plots are presented (**C**). The percentage of cell death, indicated by Annexin V and PI-positive labeling, was quantified by flow cytometry and is depicted (**D**). The data represent the means ± standard deviation (SD) of five independent experiments ($n = 5$) and are displayed in each column. Statistical significance was determined, with *** indicating $p < 0.01$. The acetylation level of AIF was analyzed by western blot using an anti-AIF-K295^{ac} antibody (**E**). **F** SK-N-SH cells were pre-treated with DMSO or the SIRT1-specific activator SRT1720 at a concentration of 10 μM for 12 h. Subsequently, the cells were untreated or exposed to MNNG. A CCK-8 assay was performed to measure cell viability as indicated time. The data represent the means of five independent experiments ($n = 5$) ± SD and are shown in each column. ***$p < 0.01$. **G** Effect of pharmacological modulation of SIRT1 on the infarct volume after MCAO was assessed. SIRT1 activator SRT1720 (200 mg/kg) dissolved in PBS or PBS (vehicle) was administered by intraperitoneal route 12 h before MCAO. The size of the MCAO-induced infarct was measured by triphenyl tetrazolium chloride (TTC) staining after MCAO (4 h). The infarct size was evaluated histomorphometrically on consecutive TTC-stained brain sections throughout the infarct (right panel). The data represent the means of five independent experiments ($n = 5$) ± SD, as shown in each column. ***$p < 0.01$. (H) DNA fragmentation was determined by gel electrophoresis in the brains of mice from sham and penumbra groups after MCAO treatment with or without SRT1720 pre-injection. **I** The acetylation levels of AIF-K295 in brain tissue samples after MCAO were analyzed by western blot using anti-AIF-K295^{ac} and anti-AIF antibodies. **J** Immunoblots of nuclear translocation of AIF after MCAO. The post-nuclear (PN) and nuclear fractions (N) of samples after MCAO from (G) were prepared, α-tubulin (post-nuclear marker) and histone H3 (nuclear marker) were used to control fractionation quality and protein loading. The quantification of nuclear and post-nuclear AIF was conducted using ImageJ software. For the quantification of post-nuclear AIF, α-tubulin was used as a control, whereas Histone H3 served as the control for nuclear AIF quantification. **K** Model illustrating the role of AIF-K295 acetylation and the SIRT1-AIF axis in regulating chromatinolysis and caspase-independent programmed necrosis.

Cell viability assay

Cell viability was measured using the Cell Counting Kit-8 (CCK-8). Five thousand cells were seeded in quintuplicate (five replicates) in 96-well plates. The detailed operational procedures can be found in the "Instructions for Use" accompanying the reagent kit. Treatment was performed ~24 h after seeding, and the vehicle control was added. At the indicated time points, cells were incubated with CCK-8 solution for 2 h. The absorbance of the treated cultures was measured using a multi-well spectrophotometer at 450 nm (Mini Max™ 300 Imaging Cytometer). The results were presented as a percentage of absorbance relative to the vehicle control cultures.

Pulsed-field gel electrophoresis

Samples were prepared as previously reported[65]. Following the incubation of cells treated with necrosis inducers, the cultures were easily pelleted by centrifugation from the medium. Monolayer cells were harvested and suspended in TEEN buffer (10 mM Tris-HCl, pH 9.5, 25 mM EDTA, 5 mM EGTA, 10 mM NaCl) with 0.1% SDS and 1 mg/ml proteinase K. For tissue analysis, brain tissue was homogenized and suspended in TEEN buffer as described above. The samples were then incubated in TEEN buffer at 55 °C overnight. Following incubation, the genomic DNA was extracted using an improved Phenol-Chloroform protocol. Briefly, an equal volume of phenol: chloroform: isoamyl alcohol (25:24:1) was added to the tube and shaken gently by hand to avoid breaking the genomic DNA. Centrifuge at 4 °C for 15 min at 500 g. Carefully remove the upper aqueous phase of the centrifuged sample and transfer it to a fresh tube, ensuring that no phenol is carried over during pipetting. Then, add an equal volume of isopropanol and 1/10 volume of 3 M NaOAc based on the volume of the sample to the tube. Place the tube at −20 °C for at least 4 h to precipitate the DNA from the sample. Centrifuge the sample again at 4 °C for 15 min at 500 g to pellet the genomic DNA. Wash the genomic DNA with 70% ethanol twice. Then, dry the DNA at room temperature and dilute the genomic DNA with 25 mM Tris-EDTA buffer at 4 °C overnight. Pulsed-field gel electrophoresis was performed using the CHEF-DR® III Pulsed Field Electrophoresis System (Bio-Rad) with the following settings: Agarose: 0.8%; Buffer: 0.5X TBE; Temperature: 18 °C; Voltage: 6 V/cm; Switch time: 3 sec; Run times: 7 h, Angle: 120°. After that, the gel was stained with SYBR Green.

Mice

Sirt1 knockout CD-1 mice were described in our previous research[21]. All experiments were conducted with *Sirt1*$^{+/+}$ and *Sirt1*$^{-/-}$ littermates. Mice were housed in a specific pathogen-free animal facility on a 12 h light-dark cycle with free access to food and water.

Ethics statement

Animal use and care protocols, including all operational procedures, were approved by the Institutional Animal Care and Use Committee of Shandong University of Technology. We have complied with all relevant ethical regulations for animal use. The research team conducted continuous monitoring of the mice post-surgery. Upon the mice regaining consciousness, observations were conducted at 20 min intervals. Health assessments were based on metrics such as food and water consumption, general activity levels, respiratory patterns, and fur condition.

Ischemic stroke model

The Common carotid artery and middle cerebral artery (MCA) were exposed and permanently occluded by ligation, as previously described[36]. Cerebral ischemia was induced by 60 min of middle cerebral artery occlusion (MCAO) following an intraperitoneal injection of chloral hydrate at a dose of 400 mg/kg. Rectal temperature was maintained at 36.5 ± 0.5 °C during surgery using an automated temperature control feedback system. A midline ventral neck incision was made, and unilateral MCAO was performed by inserting a 0.14 mm monofilament into the right internal carotid artery, 4 mm from the internal carotid/pterygopalatine artery bifurcation via an external carotid artery stump. Sham-operated animals underwent the same surgical procedure, but the suture was not advanced into the internal carotid artery. Mouse brain matrices were used to partition mouse brain tissue into coronal sections. Infarct size was measured by TTC (2,3,5-triphenyltetrazolium chloride) staining at 37 °C for 15 min. The infarct volume ratio was then determined for each coronal section using the formula: Infarct volume ratio = (sum of white ischemic area in each section) / (sum of brain slice area in each section) x 100%. We selected a small sample size ($n = 5$) because the *Sirt1* knockout or its activation through SRT1720 was evaluated in vivo for the first time in the present study, and therefore, the initial intention was to gather basic evidence regarding the use of these data in more complex experimental designs. The animals were included in the study if they underwent successful middle cerebral artery occlusion (MCAO), characterized by a reduction in cerebral blood flow of 60% or more, as measured by laser Doppler flowmetry. Animals were excluded if the insertion of the thread resulted in perforation of the vessel wall, if the silicon tip of the thread became dislodged during surgery, or if the animal died prematurely, preventing the collection of histological data. The experiment was conducted using a randomized design. Following genotyping, healthy 6–8 weeks old wild-type (WT) and *Sirt1* knockout (KO) mice of the same sex were assigned to one of four groups: male-WT, male-KO, female-WT, and female-KO. The mice in each group were assigned

identification numbers and subsequently divided into sub-groups through randomization using the RAND () function in Microsoft Excel. According to the above random number, MCAO were performed. Animals of the same sex in the same cage and with similar body weight were used as the compatibility group. After the allocation, the number of animals in each group was equal, the weight of each group was similar, so as to minimize potential confounders. Different investigators were involved as follows: a first investigator administered grouping and the treatment. A second investigator performed the surgical procedure, while a third investigator assessed TTC staining and sample collection. Humane endpoints were established to include continuous bleeding, irregular respiration, sustained body temperature below 34 °C, and ongoing tonic seizures occurring during or after the surgical procedure. The evaluation and data analysis results were entered according to the corresponding numbers of each group.

Statistics and reproducibility

All statistical analyses were performed using two-tailed Student's *t*-tests in Microsoft Excel. The results are expressed as mean ± standard deviation (SD), as indicated in the figure legends. The "*n*" represents the number of experimental replications, as shown in the figure legends. *p*-values are indicated in figure legends, with $p < 0.01$ considered statistically significant. To ensure adequate power to detect the effect, at least 5 independent tests were performed for all molecular biochemistry studies, and at least 5 different litters were used for animal studies. Experiments for quantification were performed in a blinded fashion. No data points were excluded. All data points were collected based on successful experiments. Data from animal model assumptions were checked using the Shapiro-Wilk normality test for homogeneity of variance and by visual inspection of residual and fitted value plots. If the assumptions were not met, we will revise experimental design: repeated measures or clustered data would require advanced methods (e.g., mixed-effects models in R/SPSS).

Reagent availability

All reagents generated in this study will be distributed upon request.

Reporting summary

Further information on research design is available in the Nature Portfolio Reporting Summary linked to this article.

Data availability

All relevant data are included in the manuscript and its Additional files. No data have been deposited in public databases. Uncropped and unedited blot/gel images are shown in Supplementary Figs. S5–S13. All numerical source data for graphs and charts are included in Supplementary Data 1. Gating strategy for all flow cytometry plots are included in Supplementary Data 2. All other data are available from the corresponding author on reasonable request.

Received: 8 September 2024; Accepted: 19 May 2025;
Published online: 27 May 2025

References

1. Vanden Berghe, T., Linkermann, A., Jouan-Lanhouet, S., Walczak, H. & Vandenabeele, P. Regulated necrosis: the expanding network of non-apoptotic cell death pathways. *Nat. Rev. Mol. Cell Biol.* **15**, 135–147 (2014).
2. Kim, E. H., Wong, S. W. & Martinez, J. Programmed necrosis and disease:we interrupt your regular programming to bring you necroinflammation. *Cell Death Differ.* **26**, 25–40 (2019).
3. Conrad, M., Angeli, J. P., Vandenabeele, P. & Stockwell, B. R. Regulated necrosis: disease relevance and therapeutic opportunities. *Nat. Rev. Drug Discov.* **15**, 348–366 (2016).
4. Andrabi, S. A., Dawson, T. M. & Dawson, V. L. Mitochondrial and nuclear cross talk in cell death: parthanatos. *Ann. N. Y Acad. Sci.* **1147**, 233–241 (2008).
5. Fatokun, A. A., Dawson, V. L. & Dawson, T. M. Parthanatos: mitochondrial-linked mechanisms and therapeutic opportunities. *Br. J. Pharm.* **171**, 2000–2016 (2014).
6. Strom, C. E. et al. Poly (ADP-ribose) polymerase (PARP) is not involved in base excision repair but PARP inhibition traps a single-strand intermediate. *Nucleic Acids Res* **39**, 3166–3175 (2011).
7. Delavallee, L., Cabon, L., Galan-Malo, P., Lorenzo, H. K. & Susin, S. A. AIF-mediated caspase-independent necroptosis: a new chance for targeted therapeutics. *IUBMB Life* **63**, 221–232 (2011).
8. Xie, Z. et al. Cathepsin B in programmed cell death machinery: mechanisms of execution and regulatory pathways. *Cell Death Dis.* **14**, 255 (2023).
9. Sun, L. et al. Mixed lineage kinase domain-like protein mediates necrosis signaling downstream of RIP3 kinase. *Cell* **148**, 213–227 (2012).
10. Artus, C. et al. AIF promotes chromatinolysis and caspase-independent programmed necrosis by interacting with histone H2AX. *EMBO J.* **29**, 1585–1599 (2010).
11. Wang, Y. et al. Poly(ADP-ribose) (PAR) binding to apoptosis-inducing factor is critical for PAR polymerase-1-dependent cell death (parthanatos). *Sci. Signal* **4**, ra20 (2011).
12. Zhu, C. et al. Apoptosis-inducing factor is a major contributor to neuronal loss induced by neonatal cerebral hypoxia-ischemia. *Cell Death Differ.* **14**, 775–784 (2007).
13. Susin, S. A. et al. Molecular characterization of mitochondrial apoptosis-inducing factor. *Nature* **397**, 441–446 (1999).
14. Park, H. et al. PAAN/MIF nuclease inhibition prevents neurodegeneration in Parkinson's disease. *Cell* **185**, 1943–1959.e1921 (2022).
15. Bordone, L. & Guarente, L. Calorie restriction, SIRT1 and metabolism: understanding longevity. *Nat. Rev. Mol. Cell Biol.* **6**, 298–305 (2005).
16. Guarente, L. Sir2 links chromatin silencing, metabolism, and aging. *Genes Dev.* **14**, 1021–1026 (2000).
17. Brunet, A. et al. Stress-dependent regulation of FOXO transcription factors by the SIRT1 deacetylase. *Science* **303**, 2011–2015 (2004).
18. Haigis, M. C. & Sinclair, D. A. Mammalian sirtuins: biological insights and disease relevance. *Annu Rev. Pathol.* **5**, 253–295 (2010).
19. Vaziri, H. et al. hSIR2(SIRT1) functions as an NAD-dependent p53 deacetylase. *Cell* **107**, 149–159 (2001).
20. Wang, C. et al. Interactions between E2F1 and SirT1 regulate apoptotic response to DNA damage. *Nat. Cell Biol.* **8**, 1025–1031 (2006).
21. Shan, P. et al. SIRT1 functions as a negative regulator of Eukaryotic poly(A)RNA transport. *Curr. Biol.* **27**, 2271–2284.e2275 (2017).
22. Dong, S. et al. The REGgamma proteasome regulates hepatic lipid metabolism through inhibition of autophagy. *Cell Metab.* **18**, 380–391 (2013).
23. Luna, A., Aladjem, M. I. & Kohn, K. W. SIRT1/PARP1 crosstalk: connecting DNA damage and metabolism. *Genome Integr.* **4**, 6 (2013).
24. Kolthur-Seetharam, U. et al. Control of AIF-mediated cell death by the functional interplay of SIRT1 and PARP-1 in response to DNA damage. *Cell Cycle* **5**, 873–877 (2006).
25. Rajamohan, S. B. et al. SIRT1 promotes cell survival under stress by deacetylation-dependent deactivation of poly(ADP-ribose) polymerase 1. *Mol. Cell Biol.* **29**, 4116–4129 (2009).
26. Liang, S. P. et al. Activated SIRT1 contributes to DPT-induced glioma cell parthanatos by upregulation of NOX2 and NAT10. *Acta Pharm. Sin.* **44**, 2125–2138 (2023).
27. Seiler, A. et al. Glutathione peroxidase 4 senses and translates oxidative stress into 12/15-lipoxygenase dependent- and AIF-mediated cell death. *Cell Metab.* **8**, 237–248 (2008).
28. Baritaud, M., Boujrad, H., Lorenzo, H. K., Krantic, S. & Susin, S. A. Histone H2AX: the missing link in AIF-mediated caspase-independent programmed necrosis. *Cell Cycle* **9**, 3166–3173 (2010).

29. Daugas, E. et al. Mitochondrio-nuclear translocation of AIF in apoptosis and necrosis. *FASEB J.* **14**, 729–739 (2000).
30. Zhu, C. et al. Cyclophilin A participates in the nuclear translocation of apoptosis-inducing factor in neurons after cerebral hypoxia-ischemia. *J. Exp. Med.* **204**, 1741–1748 (2007).
31. Lanneau, D., de Thonel, A., Maurel, S., Didelot, C. & Garrido, C. Apoptosis versus cell differentiation: role of heat shock proteins HSP90, HSP70 and HSP27. *Prion* **1**, 53–60 (2007).
32. Ye, H. et al. DNA binding is required for the apoptogenic action of apoptosis inducing factor. *Nat. Struct. Biol.* **9**, 680–684 (2002).
33. Cande, C. et al. AIF and cyclophilin A cooperate in apoptosis-associated chromatinolysis. *Oncogene* **23**, 1514–1521 (2004).
34. Wang, Y. et al. A nuclease that mediates cell death induced by DNA damage and poly(ADP-ribose) polymerase-1. *Science* **354**, aad6872 (2016).
35. Baritaud, M. et al. AIF-mediated caspase-independent necroptosis requires ATM and DNA-PK-induced histone H2AX Ser139 phosphorylation. *Cell Death Dis.* **3**, e390 (2012).
36. Chiang, T., Messing, R. O., Chou, W. H. Mouse model of middle cerebral artery occlusion. *J. Vis. Exp.* **13**, 2761 (2011).
37. Degterev, A. et al. Chemical inhibitor of nonapoptotic cell death with therapeutic potential for ischemic brain injury. *Nat. Chem. Biol.* **1**, 112–119 (2005).
38. Li, Y. & Zhang, J. Animal models of stroke. *Anim. Model Exp. Med* **4**, 204–219 (2021).
39. Nagasawa, H. & Kogure, K. Correlation between cerebral blood flow and histologic changes in a new rat model of middle cerebral artery occlusion. *Stroke* **20**, 1037–1043 (1989).
40. McCullough, L. D., Zeng, Z., Blizzard, K. K., Debchoudhury, I. & Hurn, P. D. Ischemic nitric oxide and poly (ADP-ribose) polymerase-1 in cerebral ischemia: male toxicity, female protection. *J. Cereb. Blood Flow. Metab.* **25**, 502–512 (2005).
41. Xu, Y., Huang, S., Liu, Z. G. & Han, J. Poly(ADP-ribose) polymerase-1 signaling to mitochondria in necrotic cell death requires RIP1/TRAF2-mediated JNK1 activation. *J. Biol. Chem.* **281**, 8788–8795 (2006).
42. Cabon, L. et al. BID regulates AIF-mediated caspase-independent necroptosis by promoting BAX activation. *Cell Death Differ.* **19**, 245–256 (2012).
43. Yu, S. W. et al. Mediation of poly(ADP-ribose) polymerase-1-dependent cell death by apoptosis-inducing factor. *Science* **297**, 259–263 (2002).
44. Bano, D. & Prehn, J. H. M. Apoptosis-inducing factor (AIF) in physiology and disease: the tale of repented natural born Killer. *EBioMedicine* **30**, 29–37 (2018).
45. Hangen, E. et al. Interaction between AIF and CHCHD4 regulates respiratory chain biogenesis. *Mol. Cell* **58**, 1001–1014 (2015).
46. Moubarak, R. S. et al. Sequential activation of poly(ADP-ribose) polymerase 1, calpains, and Bax is essential in apoptosis-inducing factor-mediated programmed necrosis. *Mol. Cell Biol.* **27**, 4844–4862 (2007).
47. Wang, H. F. et al. Endoplasmic reticulum stress regulates oxygen-glucose deprivation-induced parthanatos in human SH-SY5Y cells via improvement of intracellular ROS. *CNS Neurosci. Ther.* **24**, 29–38 (2018).
48. North, B. J., Marshall, B. L., Borra, M. T., Denu, J. M. & Verdin, E. The human Sir2 ortholog, SIRT2, is an NAD+-dependent tubulin deacetylase. *Mol. Cell* **11**, 437–444 (2003).
49. Doti, N. et al. Inhibition of the AIF/CypA complex protects against intrinsic death pathways induced by oxidative stress. *Cell Death Dis.* **5**, e993 (2014).
50. Eliasson, M. J. et al. Poly(ADP-ribose) polymerase gene disruption renders mice resistant to cerebral ischemia. *Nat. Med.* **3**, 1089–1095 (1997).
51. Culmsee, C. et al. Apoptosis-inducing factor triggered by poly(ADP-ribose) polymerase and Bid mediates neuronal cell death after oxygen-glucose deprivation and focal cerebral ischemia. *J. Neurosci.* **25**, 10262–10272 (2005).
52. Hernandez-Jimenez, M. et al. Silent information regulator 1 protects the brain against cerebral ischemic damage. *Stroke* **44**, 2333–2337 (2013).
53. Yu, S. W. et al. Outer mitochondrial membrane localization of apoptosis-inducing factor: mechanistic implications for release. *ASN Neuro* **1**, e00021 (2009).
54. Novo, N. et al. Beyond a platform protein for the degradosome assembly: the apoptosis-Inducing Factor as an efficient nuclease involved in chromatinolysis. *PNAS Nexus* **2**, pgac312 (2023).
55. Montague, J. W., Hughes, F. M. Jr & Cidlowski, J. A. Native recombinant cyclophilins A, B, and C degrade DNA independently of peptidylprolyl cis-trans-isomerase activity. *J. Biol. Chem.* **272**, 6677–6684 (1997).
56. Hu, J. X. et al. Macrophage migration inhibitory factor (MIF) acetylation protects neurons from ischemic injury. *Cell Death Dis.* **13**, 466 (2022).
57. Koronowski, K. B. & Perez-Pinzon, M. A. Sirt1 in cerebral ischemia. *Brain Circ.* **1**, 69–78 (2015).
58. Yu, W., Mechawar, N., Krantic, S. & Quirion, R. Evidence for the involvement of apoptosis-inducing factor-mediated caspase-independent neuronal death in Alzheimer disease. *Am. J. Pathol.* **176**, 2209–2218 (2010).
59. Burguillos, M. A. et al. Apoptosis-inducing factor mediates dopaminergic cell death in response to LPS-induced inflammatory stimulus: evidence in Parkinson's disease patients. *Neurobiol. Dis.* **41**, 177–188 (2011).
60. Reijonen, S., Putkonen, N., Norremolle, A., Lindholm, D. & Korhonen, L. Inhibition of endoplasmic reticulum stress counteracts neuronal cell death and protein aggregation caused by N-terminal mutant huntingtin proteins. *Exp. Cell Res* **314**, 950–960 (2008).
61. Oh, Y. K., Shin, K. S. & Kang, S. J. AIF translocates to the nucleus in the spinal motor neurons in a mouse model of ALS. *Neurosci. Lett.* **406**, 205–210 (2006).
62. Hubbard, B. P. et al. Evidence for a common mechanism of SIRT1 regulation by allosteric activators. *Science* **339**, 1216–1219 (2013).
63. Zhang, M. et al. HDAC6 regulates DNA damage response via deacetylating MLH1. *J. Biol. Chem.* **294**, 5813–5826 (2019).
64. Kim, J. E., Chen, J. & Lou, Z. DBC1 is a negative regulator of SIRT1. *Nature* **451**, 583–586 (2008).
65. Walker, P. R., Leblanc, J., Smith, B., Pandey, S. & Sikorska, M. Detection of DNA fragmentation and endonucleases in apoptosis. *Methods* **17**, 329–338 (1999).

Acknowledgements

This work was supported by the National Natural Science Foundation of China (32170784, 32170707, 32470803 and 31900552). We thank Professor Zhiyong Li from the Marine Biotechnology Laboratory at Shanghai Jiao Tong University for providing the instrument for pulsed-field gel electrophoresis and for the technical support in the analysis of large-scale DNA fragmentation.

Author contributions

C.H., J.G. performed most of the experiments; S.Z. and C.W. interpreted data and wrote the manuscript; P.S., T.Z., Z.Z, Xiaoyu Zhang, M.L., Xiaoxia Zhang, and D.C. helped with all experiments; B.H., D.J., and M.Z. supervised the study and reviewed the manuscript. All authors have read and approved the final manuscript.

Competing interests

The authors declare no competing interest.

Additional information

Supplementary information The online version contains supplementary material available at https://doi.org/10.1038/s42003-025-08255-w.

Correspondence and requests for materials should be addressed to Chuangui Wang or Shengping Zhang.

Peer review information *Communications Biology* thanks the anonymous reviewers for their contribution to the peer review of this work. Primary Handling Editors: Jasmine Pan and Benjamin Bessieres. A peer review file is available.